Computer Modeling in Engineering & Sciences

Tech Science Press

https://doi.org/10.32604/cmes.2026.082608

ARTICLE

Instantaneous Mobility Indicators for Risk Management in Wind Farms: A Computer Modeling Approach

Guglielmo D'Amico[1,*], Edoardo Lui[2] and Filippo Petroni[1]

[1]Department of Economics, University G. d'Annunzio, Pescara, Italy
[2]Department of Physics, University of Genoa, Genoa, Italy

*Corresponding Author: Guglielmo D'Amico. Email: guglielmo.damico@unich.it

Received: 19 March 2026; Accepted: 29 June 2026; Published: 27 July 2026

ABSTRACT: This paper develops an operational framework for short-horizon risk management in multistate stochastic systems, with application to wind farm performance. We focus on instantaneous mobility-based indicators derived from finite-state continuous-time Markov chains, which capture the local propensity of a system to transition between states. Unlike classical reliability and availability measures, these indicators provide a dynamic description of system behavior. The indicators are interpreted as policy signals to support decision-making under budget constraints. We introduce a state-conditional expected short-horizon loss, representing non-production risk, and use it to evaluate ranking-based intervention strategies. The framework is applied to a global dataset of wind farms. Results show that mobility-based indicators, especially those related to transition intensity, outperform standard availability proxies in identifying high-risk conditions and concentrating expected losses among top-ranked observations. This supports their use as effective tools for data-driven, policy-oriented risk management.

KEYWORDS: Wind farms; operational risk; non-production risk; Markov processes; semi-Markov processes; instantaneous failure and repair rates; ROCOF; ROCOR; ROI; mobility; energy-at-risk; revenue-at-risk

1 Introduction

The literature on reliability theory and stochastic modeling of complex systems is vast and continuously evolving, driven by the need to characterize system behavior, quantify risk, and support operational decision-making in engineering applications; see, among others [1–3]. In this framework, reliability is inherently probabilistic, as it concerns the random evolution of a system over time, and any rigorous analysis must start from an explicit stochastic description of the system dynamics.

A central modeling paradigm is that of multistate systems, in which system operation is represented by a finite state space with random transitions [4]. Continuous-time Markov and semi-Markov processes play a central role in this context; see, e.g., [5,6]. The former type imposes exponential sojourn times, the latter allows for general state-dependent holding-time distributions, offering increased modeling flexibility and practical relevance.

In this context, a comprehensive understanding of system behavior requires multiple indicators. Classical cumulative measures include the reliability and availability functions, which have been extensively studied for Markov systems [7] and extended to semi-Markov frameworks [8,9]. Further generalizations include interval reliability measures [10,11], discrete-time counterparts [12,13], and sequential reliability concepts [14,15]. These indicators quantify system behavior over finite horizons but do not directly describe the instantaneous dynamics of transitions.

Instantaneous reliability measures address this limitation by characterizing the local propensity of a system to experience specific events. Among them, the Rate of Occurrence of Failures (ROCOF), defined as the time derivative of the expected number of failures, has attracted significant attention. For multistate continuous-time Markov chains, explicit ROCOF formulas were derived by [16–18], later extended to semi-Markov settings by [19,20]. Higher-order generalizations and systematic treatments of ROCOF-type indicators can be found in [21,22].

Nevertheless, ROCOF alone does not fully characterize the instantaneous behavior of a system. In [23], the Rate of Occurrence of Repairs (ROCOR), the Rate of Inoccurrence (ROI), and the Total Mobility Rate (TMR) have been included. These quantities jointly describe the instantaneous tendency of a system to fail, recover, or persist in its current condition, and satisfy structural identities that hold independently of the chosen partition of the state space.

The present paper builds on this theoretical framework and shifts the focus toward an empirical and operational perspective. In particular, we investigate how mobility-based indicators can be used as *policy signals* for short-horizon risk management and site-level prioritization. We consider policies as decision rules that trigger interventions based on observed indicator values, under explicit budget constraints.

In this sense, our framework connects to the theory of ranking risk minimization [24]. In particular, it is convenient to work with a short-horizon state-conditional expected loss for operational decision-making. Expected non-production loss can be interpreted as a target functional inducing a pairwise ordering structure over sites, analogously to bipartite ranking formulations.

Methodologically, we model wind-speed regime dynamics through a finite-state CTMC and extract instantaneous mobility indicators from the generator matrix. These indicators are then interpreted as policy signals for operational decision-making and evaluated against a state-conditional expected short-horizon production loss. This methodology is applied to a global dataset of wind farms. Using expected short-horizon production loss as a target variable, we evaluate the predictive and operational value of different signals through classification and ranking criteria, including the Area Under the ROC Curve (AUC) and lift curves. The AUC is widely used as a threshold-independent measure of discriminative ability (see, e.g., [25,26]) and admits an interpretation as the probability that a randomly chosen positive instance is ranked above a randomly chosen negative one [27]. In the context of ranking-based decision rules, it provides a natural aggregate measure of discrimination performance across operating conditions.

The empirical results show that mobility-based indicators—particularly those related to transition intensity—provide superior discrimination and capture a larger share of expected loss under constrained intervention budgets, compared to standard availability proxy. In operational terms, lift curves illustrate how the expected loss concentrates within the highest-ranked fraction of sites or decision times. A lift curve is constructed by ordering observations according to the model's predicted risk and then plotting the cumulative share of total expected loss captured as an increasing fraction of the top-ranked observations considered [28,29]. The random baseline corresponds to a linear curve, indicating that loss is uniformly distributed across the ranking. Deviations above this benchmark indicate that the model successfully concentrates high-loss events at the top of the ranking. Lift curves therefore directly link ranking performance to actionable budget allocation strategies under resource constraints, as steeper initial segments indicate signals that capture a disproportionately large share of expected loss while acting on only a limited fraction of sites or intervention opportunities.

Finally, we stress the fact taht the empirical analysis should be interpreted as an indicator-oriented comparison rather than as a formal predictive validation exercise. The aim of the paper is not to perform statistical inference on a forecasting model, but to describe and assess the operational behavior of the proposed mobility-based indicators relative to benchmark signals. AUC and lift curves are therefore used as descriptive ranking-performance measures, designed to evaluate how effectively each indicator prioritizes observations associated with larger short-horizon expected losses. This interpretation is consistent with the decision-support perspective of the study, in which the main objective is to compare the usefulness of alternative signals for risk-aware short-horizon prioritization under budget constraints.

The paper is organized as follows. Sections 2 and 3 recall the relevant theoretical framework and instantaneous indicators. Section 4 introduces quantitative measures of non-production risk over a horizon. Section 5 describes the data, estimation procedures and empirical design while Section 6 presents the policy-oriented numerical results and cross-site comparisons. Section 7 concludes and outlines directions for further research.

2 Modeling Framework

The objective of the present work is to investigate whether instantaneous mobility indicators extracted from a stochastic model of wind dynamics can be used as operational signals for short-horizon risk management in wind farms. In order to formalize the transition structure of wind-speed regimes and to derive interpretable indicators of regime switching, in this Section we present a finite-state CTMC representation of the wind-speed process. Section 2.1 introduces the CTMC representation of wind-speed regimes and the associated wind-to-power mapping at the farm level. Section 2.2 then defines the partition of the state space into working and failure sets, which allows the stochastic wind dynamics to be linked to operational availability and non-production risk.

Within this framework, wind dynamics, power production, and operational availability can be linked in a coherent probabilistic model. The resulting representation allows us to construct loss functionals associated with non-production exposure and to evaluate the predictive and operational value of mobility-based indicators in the empirical analysis developed in the subsequent Sections.

2.1 Wind Farm as a Multi-State Stochastic System

Let $\{X(t),\ t \geq 0\}$ be a time-homogeneous continuous-time Markov chain (CTMC) with finite state space $E = \{1, 2, \ldots, s\}$ on a filtered probability space $(\Omega, \mathcal{F}, \{\mathcal{F}_t\}, \mathbb{P})$. In the present work, $X(t)$ is introduced to model the stochastic evolution of the *wind-speed regime* at the wind farm site (or at hub height), and *not* the electrical production itself. Each state $i \in E$ corresponds to a wind-speed class (regime) and can be interpreted as the event

$$X(t) = i \quad \Longleftrightarrow \quad V(t) \in I_i,$$

where $V(t)$ denotes the (continuous) wind-speed process and $\{I_i\}_{i\in E}$ is a measurable partition of $\mathbb{R}_+$ into s disjoint intervals. Such analyses are commonly adopted in reliability modeling, particularly in the context of availability analysis [30]. The probabilistic evolution of the regimes is described by the transition probability functions

$$P_{i,j}(t) := \mathbb{P}[X(t) = j \mid X(0) = i], \qquad i, j \in E,\ t \geq 0, \tag{1}$$

and by the initial distribution $\alpha_i := \mathbb{P}[X(0) = i]$, $i \in E$, with $\sum_{i\in E} \alpha_i = 1$.

In the time-homogeneous setting, the dynamics are fully characterized by the generator matrix $\mathbf{Q} = (q_{i,j})_{i,j\in E}$, whose off-diagonal elements satisfy $q_{i,j} \geq 0$ for $i \neq j$ and whose diagonal elements are given by

$$q_{i,i} = -\sum_{j\in E,\, j\neq i} q_{i,j}, \qquad i \in E. \tag{2}$$

The generator admits the standard interpretation in terms of instantaneous transition intensities:

$$q_{i,j} = \lim_{t\to 0^+} \frac{P_{i,j}(t)}{t}, \qquad i \neq j, \qquad q_{i,i} = \lim_{t\to 0^+} \frac{P_{i,i}(t) - 1}{t}. \tag{3}$$

Let $\mathbf{P}(t) = (P_{i,j}(t))_{i,j\in E}$ denote the transition probability matrix. Then $\mathbf{P}(t)$ is the unique solution to the forward and backward Kolmogorov equations,

$$\dot{\mathbf{P}}(t) = \mathbf{P}(t)\mathbf{Q}, \qquad \dot{\mathbf{P}}(t) = \mathbf{Q}\mathbf{P}(t), \qquad \mathbf{P}(0) = \mathbf{I}, \tag{4}$$

and therefore

$$\mathbf{P}(t) = e^{\mathbf{Q}t}, \qquad t \geq 0. \tag{5}$$

Finally, the unconditional state probabilities $p_j(t) := \mathbb{P}[X(t) = j]$ are obtained as

$$p_j(t) = \sum_{i\in E} \alpha_i P_{i,j}(t), \qquad \text{equivalently}\, p(t) = \alpha \cdot e^{\mathbf{Q}t}. \tag{6}$$

The CTMC $\{X(t)\}$ provides a regime-switching representation of wind-speed dynamics.

Consider a wind farm composed of NT turbines. We introduce electrical power of the single turbine $j \in \{1, \ldots, NT\}$ through a state-dependent mapping

$$g^{(j)} : E \to \mathbb{R}_+, \qquad g^{(j)}(i) = g(i)(1 + \epsilon^{(j)}(i)), \tag{7}$$

$$i \mapsto g^{(j)}(i), \qquad \forall\, j \in \{1, \ldots, NT\} \tag{8}$$

where $g(i)$ denotes the representative ideal turbine power associated with wind regime i, while $\epsilon^{(j)}(i)$ represents a state and turbine-dependent perturbation term. Specifically, it depends on the wind regime i and on the turbine index j, and accounts for deviations from the ideal reference power $g(i)$ due, for instance, to local terrain conditions, air pressure variations, topographical effects, and other site-specific environmental factors. The mapping $g(\cdot)$ is constructed from the turbine power curve and in Table 1 $g(i)$ is normalized by the maximum electrical power (typically 2 MW [31]) by assigning a representative wind-speed to each interval I_i (e.g., arithmetical mean) or, when SCADA data are available, by estimating $g(i)$ directly as the conditional mean power given $X(t) = i$.

Table 1: State-dependent power mapping.

State	**0**	**1**	**2**	**3**	**4**	**5**	**6**	**7**	**8**	**9**	**10**
Velocity (m/s)	0–2	2–4	4–6	6–8	8–10	10–12	12–14	14–16	16–18	18–20	20–22
$g(i)$	0.00	0.00	0.20	0.35	0.50	0.65	0.80	0.92	1.00	0.00	0.00

From the definition of the electrical power $g^{(j)}(i)$ in Eq. (7), the instantaneous power of the farm is modeled as

$$Pow_{\text{farm}}(t) = \sum_{i\in E}\sum_{j\in NT} g(X(t))(1+\epsilon^{(j)}\,(X(t))\mathbb{I}_{\{X(t)=i\}} \tag{9}$$

where $\mathbb{I}_{\{X(t)=i\}}$ represents the indicator function of the state i.

In the present paper, we neglect the perturbation effects due to $\epsilon^{(j)}\,(i)$, as detailed information on turbine and state-specific deviations was not available. Accordingly, we assume the ideal case $\epsilon^{(j)}\,(i) = 0$ for all $i \in E$ and for all $j \in \{1, \dots, NT\}$. Therefore, in the following, the turbine-specific power mapping reduces to $g^{(j)}(i) = g(i)$, meaning that all turbines are assumed to share the same state-dependent representative power curve. The assumption $\epsilon^{(j)}\,(i) = 0$ should therefore be understood as a data-driven simplification rather than as a structural restriction of the proposed methodology. In a more detailed site-specific implementation, the perturbation term $\epsilon^{(j)}\,(i)$ could be calibrated directly from turbine-level information, including turbine coordinates, hub height, rotor diameter, terrain and air-density corrections, local wind-direction effects, and wake interactions. Detailed modelling approaches for such effects are available in the wind-energy literature, including analytical wake interaction models and layout-dependent corrections in [32]. If such wind-farm-specific information were available, it could be incorporated directly into the turbine-specific production map $g^{(j)}(i)$. Importantly, the proposed CTMC-based risk-management framework would remain unchanged: the only modification would consist in replacing the representative mapping $g(i)$ with the calibrated turbine-specific functions $g^{(j)}(i)$, while the estimation of the transition structure, the construction of mobility indicators, and the policy-evaluation layer would remain valid.

Therefore, Eq. (9) becomes

$$Pow_{\text{farm}}(t) = NT\,g(X(t)) \tag{10}$$

Hence, for any time horizon $H > 0$, the (random) energy produced by the farm over $[0, H]$ is given by the functional

$$E_{\text{farm}}(H) = \int_0^H Pow_{\text{farm}}(t)\,\mathrm{d}t = NT\int_0^H g(X(t))\,\mathrm{d}t. \tag{11}$$

Eqs. (9)–(11) provide the required connection between (i) a stochastic model for wind-speed regimes, described by the CTMC with generator $\mathbf{Q}$, and (ii) the induced stochastic dynamics of power and energy at the farm level, described as functionals of $\{X(t)\}$ through the mapping $g(\cdot)$. This separation will allow us, in subsequent Sections, to define non-production losses and risk measures by combining state probabilities (6) with the output map (7).

2.2 Working vs. Failure Sets and Operational Mapping

Let $E = \{1, 2, \dots, s\}$ denote the finite state space of the CTMC $\{X(t), t \geq 0\}$ modeling wind-speed regimes, as introduced in Section 2.1. In order to connect wind-speed regime dynamics with operational availability and non-production risk, we introduce a partition of the state space based on the operational status of the wind farm.

From Table 1, we partition E into two non-empty, disjoint subsets

$$W = \{\text{working states}\}, \qquad F = \{\text{failure (non-operational) states}\}, \tag{12}$$

such that

$$W \cup F = E, \qquad W \cap F = \varnothing.$$

The classification is performed at the level of wind-speed regimes and reflects the operational capability of the farm under those regimes. States in W correspond to wind conditions under which the farm is operational and capable of producing electrical power, thus $g(i) > 0$ for $i \in W$. On the other hand, states in F correspond to wind conditions under which production is not feasible and the farm is effectively non-operational, thus $g(i) = 0$ for all $i \in F$. In particular, states $i \in \{9, 10\}$ are included in the failure set F, since the corresponding wind-speed ranges exceed the turbine cut-out velocity. This definition is deliberately abstract and does not attribute failure to specific mechanical components; rather, it captures operational unavailability induced by the wind-speed regime itself.

Define the indicator functions of the working and failure set as

$$\mathbb{I}_W(i) = \begin{cases} 1, & i \in W, \\ 0, & i \in F, \end{cases} \qquad \mathbb{I}_F(i) = \begin{cases} 0, & i \in W, \\ 1, & i \in F, \end{cases} \qquad i \in E. \tag{13}$$

Then the instantaneous operational status of the wind farm at time t can be represented by the random variable $\mathbb{I}_W(X(t))$. In particular, the probability that the system is operational at time t is given by

$$A(t) := \mathbb{P}[X(t) \in W] = \sum_{j \in W} p_j(t). \tag{14}$$

Eq. (14) provides a time-dependent notion of availability, derived directly from the wind-regime CTMC.

Finally, from the partition of E into W and F disjoint subsets, the farm-level power process defined in (9) can be written as

$$Pow_{\text{farm}}(t) = NT\, g(X(t)) = NT\, g(X(t))\, \mathbb{I}_W(X(t)), \tag{15}$$

where the indicator explicitly highlights the dependence on the operational status.

The partition (12) induces a natural classification of transitions of the CTMC into three categories: transitions from W to F (loss of operability), transitions from F to W (recovery of operability), and transitions within the same subset (persistence of the operational status). Formally, the generator matrix Q can be decomposed into blocks corresponding to these transition types. This decomposition will play a central role in the definition of instantaneous reliability and mobility indicators, as it allows us to express failure, repair, and persistence rates directly in terms of the generator and the state probabilities.

By defining working and failure sets at the level of wind-speed regimes, the model separates the stochastic dynamics of wind from the operational consequences for the wind farm. This separation is essential for risk management: it enables the quantification of time-dependent availability, non-production, and operational risk as functionals of the CTMC, while maintaining a clear and mathematically rigorous link between wind-speed regime transitions and operational outcomes.

3 Instantaneous Reliability and Mobility Indicators

The stochastic framework introduced in Section 2 provides a probabilistic description of the evolution of wind-speed regimes through a CTMC. While this representation fully characterizes the dynamics of the system, operational decision-making requires quantities that capture the local transition behavior of the process. In particular, for risk-aware operational policies it is important to quantify the instantaneous tendency of the system to change regime, lose operability, or recover from adverse conditions.

For this purpose, we consider a class of *instantaneous mobility indicators* derived from the transition structure of the CTMC. These quantities summarize the local intensity of regime switching and provide interpretable signals describing the propensity of the system to fail, recover, or persist in its current operational state.

In the present work, these indicators are not only interpreted as descriptors of reliability dynamics, but are also used as *policy signals* for short-horizon operational risk management. In particular, they are evaluated in the empirical analysis for their ability to anticipate short-horizon non-production exposure and to support ranking-based intervention policies across wind-farm sites.

This Section recalls the instantaneous reliability and mobility indicators introduced in [23,33], restricting attention to the elements that are strictly necessary for the development of the present work. Full derivations, properties, and extensions can be found in the cited reference and are therefore omitted here.

3.1 Event-Counting Processes and Operational Transitions

Let $\{X(t), t \geq 0\}$ be the CTMC defined in Section 2, with state space E partitioned into working and failure subsets W and F. The partition induces a natural classification of transitions of the process according to their operational meaning.

We introduce the following counting processes:

- $N_f(t)$: number of transitions from W to F on the interval $[0, t]$ (loss of operability);
- $N_r(t)$: number of transitions from F to W on the interval $[0, t]$ (recovery of operability);
- $N_i(t)$: number of transitions within W or within F on the interval $[0, t]$ (persistence of the operational status).

These processes provide a stochastic representation of failure, repair, and persistence events induced by the wind-regime dynamics.

3.2 Instantaneous Failure, Repair, and Inoccurrence Rates

Following [23,33], the instantaneous reliability and mobility indicators are defined as the expected infinitesimal increments of the corresponding counting processes. First of all, the Rate of Occurrence of Failures (ROCOF) at time t is defined as

$$\mathrm{ROCOF}(t) := \lim_{\Delta t \to 0} \frac{\mathbb{E}[N_f(t+\Delta t) - N_f(t)]}{\Delta t}. \tag{16}$$

The Rate of Occurrence of Repairs (ROCOR) at time t is defined as

$$\mathrm{ROCOR}(t) := \lim_{\Delta t \to 0} \frac{\mathbb{E}[N_r(t+\Delta t) - N_r(t)]}{\Delta t}. \tag{17}$$

Finally, the Rate of Inoccurrence (ROI) at time t is defined as

$$\mathrm{ROI}(t) := \lim_{\Delta t \to 0} \frac{\mathbb{E}[N_i(t+\Delta t) - N_i(t)]}{\Delta t}. \tag{18}$$

These quantities characterize, respectively, the instantaneous propensity of the system to lose operability, to recover operability, and to persist in its current operational condition.

Under the CTMC assumptions of Section 2.1, the indicators admit closed-form expressions in terms of the generator matrix $\mathbf{Q}$ and the transition probability matrix $\mathbf{P}(t) = e^{\mathbf{Q}t}$. Specifically, letting $\alpha_i = \mathbb{P}[X(0) = i]$, one obtains (see [23,33]):

$$\mathrm{ROCOF}(t) = \sum_{i\in E}\sum_{w\in W}\sum_{f\in F}\alpha_i\, P_{i,w}(t)\, q_{w,f}, \tag{19}$$

$$\mathrm{ROCOR}(t) = \sum_{i\in E}\sum_{f\in F}\sum_{w\in W}\alpha_i\, P_{i,f}(t)\, q_{f,w}, \tag{20}$$

$$\mathrm{ROI}(t) = \sum_{i\in E}\left[\sum_{\substack{w,w'\in W\\ w'\neq w}}\alpha_i\, P_{i,w}(t)\, q_{w,w'} + \sum_{\substack{f,f'\in F\\ f'\neq f}}\alpha_i\, P_{i,f}(t)\, q_{f,f'}\right]. \tag{21}$$

These expressions highlight the role of the generator blocks associated with transitions between and within the sets W and F. In the following Sections, we will consider Eqs. (19)–(21) in the limit $t \to 0^+$.

The Total Mobility Rate (TMR) is defined as the sum

$$\mathrm{TMR}(t) := \mathrm{ROCOF}(t) + \mathrm{ROCOR}(t) + \mathrm{ROI}(t), \tag{22}$$

and measures the overall intensity of regime switching of the wind-speed regime process at time t. In the present context, TMR provides a synthetic indicator of short-term operational volatility induced by wind dynamics. A key theoretical result established in [23] concerns the structural nature of the TMR. While the individual indicators $\mathrm{ROCOF}(t)$, $\mathrm{ROCOR}(t)$, and $\mathrm{ROI}(t)$ explicitly depend on the chosen partition of the state space into working and failure sets (W, F), their sum does not.

Proposition 1: *Let $\{X(t), t \geq 0\}$ be a CTMC on a finite state space E with generator matrix* $\mathbf{Q}$, *and let (W, F) be any partition of E into two non-empty disjoint subsets. Then, for all $t \geq 0$, the Total Mobility Rate*

$$\mathrm{TMR}(t) = \mathrm{ROCOF}(t) + \mathrm{ROCOR}(t) + \mathrm{ROI}(t)$$

is independent of the specific choice of the partition (W, F).

As shown in [23], $\mathrm{TMR}(t)$ admits the alternative representation

$$\mathrm{TMR}(t) = \sum_{i\in E}\sum_{\substack{j\in E\\ j\neq i}}\alpha_i\, P_{i,i}(t)\, q_{i,j}, \tag{23}$$

which depends only on the generator matrix $\mathbf{Q}$ and on the state probabilities of the CTMC, and therefore captures the intrinsic intensity of regime switching of the underlying stochastic process.

Interpretation:

Proposition 1 shows that $\mathrm{TMR}(t)$ is an intrinsic property of the wind-speed regime dynamics and not an artifact of how operational states are classified. In the context of wind farms, this implies that TMR measures the inherent short-term volatility of wind conditions, independently of how "working" and "failure" regimes are defined. This property makes TMR particularly suitable as a robust indicator of operational risk and regime instability, and motivates its use in the risk-management framework developed in the remainder of the paper.

3.3 Role of the Indicators in the Present Work

In the original contributions [23,33], the indicators ROCOF(t), ROCOR(t), ROI(t), and TMR(t) were introduced and analyzed as dynamic descriptors of reliability and mobility in continuous-time Markov systems. Their interpretation was primarily focused on the structural characterization of regime switching and persistence properties of multi-state stochastic models.

In the present work, these indicators play a fundamentally different role. They are employed as *primitive quantities for operational risk management* in wind farm systems, where the underlying stochastic dynamics are driven by wind-speed regime transitions. In particular, the distinction between partition-dependent indicators (ROCOF, ROCOR, ROI) and the partition-invariant TMR is exploited to separate operationally induced risk from intrinsic wind volatility.

The indicators are systematically combined with the wind-to-power mapping introduced in Section 2 to construct time-dependent measures of non-production and revenue risk. In this framework, ROCOF(t) and ROCOR(t) quantify the instantaneous exposure to losses and recovery potential under a given operational classification, while TMR(t) provides a robust baseline measure of regime instability that is independent of the working–failure partition. This separation allows us to design indicator-driven maintenance and operational policies that explicitly account for both short-term risk exposure and structural uncertainty in wind dynamics, and to assess their impact on non-production risk over finite planning horizons.

4 Non-Production Risk and Policy Target

The cumulative loss variables and tail-risk measures introduced in this Section, Energy-at-Risk (EaR) and Revenue-at-Risk (RaR) are included to motivate the use of additive loss functionals of the CTMC and to clarify the link between regime transitions and downside exposure. In the empirical analysis, however, these quantities are *not* used as primary performance metrics. Instead, they provide the theoretical background for the short-horizon, state-conditional expected loss employed as the operational target in the policy evaluation layer.

This Section introduces quantitative measures of non-production risk over a finite planning horizon. Starting from the wind-speed regime CTMC and the wind-to-power mapping $g(\cdot)$, we define energy and revenue loss functionals and their associated tail-risk measures EaR and RaR. We then make the connection with instantaneous mobility indicators explicit through identities and deterministic bounds, thereby clarifying how the transition structure drives both average exposure and tail behavior.

4.1 Energy Production, Reference Production, and Loss Functionals

In what follows, we restrict attention to intervention settings arising in maintenance decision-making. Fix a planning horizon $H > 0$. As established in Section 2, the wind-speed regime is modeled by a CTMC $\{X(t), t \geq 0\}$ on a finite state space E, with generator $\mathbf{Q}$ and transition matrix $\mathbf{P}(t) = e^{\mathbf{Q}t}$. The farm power during non ideal conditions, i.e., during maintenance, is introduced as an output functional of the CTMC through a mapping $g^\star : E \to \mathbb{R}_+$, so that

$$Pow^\star_{\text{farm}}(t) = NT\, g^\star(X(t)), \qquad t \in [0, H].$$

To quantify non-production, we use the reference (or potential) power mapping $g : E \to \mathbb{R}_+$ introduced in Section 2, representing the power that would be produced in each wind-speed regime under ideal operational conditions. The corresponding reference power is

$$Pow_{\text{farm}}(t) = NT\, g(X(t)).$$

Hence, the instantaneous power gap is $P_{\text{farm}}(t) - P^{\star}_{\text{farm}}(t)$ and the *cumulative energy loss* over $[0, H]$ is defined as the random variable

$$L_E(H) := \int_0^H \left(Pow_{\text{farm}}(t) - Pow^{\star}_{\text{farm}}(t)\right) \mathrm{d}t = NT \int_0^H \left\{g(X(t)) - g^{\star}(X(t))\right\} \mathrm{d}t. \tag{24}$$

Equivalently, defining the state-dependent *instantaneous energy-loss rate*

$$c(i) := NT\big(g(i) - g^{\star}(i)\big) \geq 0, \qquad i \in E, \tag{25}$$

we can rewrite (24) as the additive functional

$$L_E(H) = \int_0^H c(X(t))\,\mathrm{d}t. \tag{26}$$

To incorporate financial exposure, let $\{\Pi(t), t \geq 0\}$ be a non-negative, locally integrable electricity price process. The *cumulative revenue loss* due to non-production is

$$L_R(H) := \int_0^H \Pi(t)\left(Pow_{\text{farm}}(t) - Pow^{\star}_{\text{farm}}(t)\right) \mathrm{d}t = \int_0^H \Pi(t)\, c(X(t))\,\mathrm{d}t. \tag{27}$$

No parametric assumption on $\Pi(\cdot)$ is required here.

4.2 Energy-at-Risk and Revenue-at-Risk

The loss variables $L_E(H)$ and $L_R(H)$ induce loss distributions that reflect both persistence in adverse regimes and the timing of transitions among wind-speed states. We measure downside exposure through quantile-based risk measures.

Let $\beta \in (0, 1)$. The EaR over $[0, H]$ at confidence level β is

$$\mathrm{EaR}_{\beta}(H) := \inf\left\{\ell \in \mathbb{R}_+ : \mathbb{P}(L_E(H) \leq \ell) \geq \beta\right\}. \tag{28}$$

The RaR over $[0, H]$ at confidence level β is

$$\mathrm{RaR}_{\beta}(H) := \inf\left\{\ell \in \mathbb{R}_+ : \mathbb{P}(L_R(H) \leq \ell) \geq \beta\right\}. \tag{29}$$

4.3 Expected Losses and State-Probability Representation

Let $p(t) = \alpha \cdot e^{\mathbf{Q}t}$ denote the row vector of state probabilities, $p_i(t) = \mathbb{P}(X(t) = i)$. Then

$$\mathbb{E}[L_E(H)] = \int_0^H \mathbb{E}[c(X(t))]\,\mathrm{d}t = \int_0^H \sum_{i \in E} p_i(t)\, c(i)\,\mathrm{d}t, \tag{30}$$

$$\mathbb{E}[L_R(H)] = \int_0^H \mathbb{E}[\Pi(t)\, c(X(t))]\,\mathrm{d}t. \tag{31}$$

For simplicity here we consider the stochastic electrical price process $\Pi(t)$ to be independent from the wind process, then

$$\mathbb{E}[L_R(H)] = \mathbb{E}[\Pi(H)] \int_0^H \sum_{i \in E} p_i(t)\, c(i)\,\mathrm{d}t. \tag{32}$$

Eqs. (30)–(32) show that average exposure is fully determined by the CTMC state probabilities and the loss-rate mapping $c(\cdot)$.

4.4 Target Variable: Short-Horizon Expected Incremental Loss

The above theoretical analysis characterize the average non-production exposure over a finite horizon in terms of the CTMC state probabilities and the loss-rate mapping. For operational decision-making, however, it is convenient to work with a short-horizon, state-conditional quantity that captures the expected loss following the currently observed regime. This motivates the definition of the policy target.

All policy signals are evaluated against a common CTMC-consistent target.

Let $\{X(t)\}_{t\geq 0}$ be a CTMC on a finite state space $E = \{1, \ldots, S\}$ with generator $\mathbf{Q}$. Let $c : E \to \mathbb{R}_+$ be a nonnegative state-dependent *loss-rate map* (non-production loss rate). Fix a short operational horizon $\Delta > 0$ (in the empirical implementation, $\Delta \in \{6, 8\}$ h). These values are chosen to represent the typical intra-day operational decision windows, over which inspection or maintenance decisions can be updated using newly observed wind-regime information. This choice is also consistent with the CTMC framework. Since CTMC entails exponentially distributed residence times, longer horizons would make the evaluation more dependent on the Markov residence-time assumption and hence more exposed to potential semi-Markov or non-Markovian effects. By focusing on short horizons, the indicators are used as local risk signals based on short-run transition behaviour. Considering $\Delta \in \{6, 8\}$ hours windows provides a sensitivity check with respect to the horizon length and avoids relying on a single arbitrary value of Δ.

The ground-truth target is defined as the conditional short-horizon expected incremental loss

$$Y(t) = \mathbb{E}\left[\int_0^{\Delta} c\big(X(t+u)\big)\,\mathrm{d}u \,\middle|\, X(t) \right]. \tag{33}$$

Conditioning on the observed state $X(t)$ is essential for policy evaluation: if one uses a stationary or near-stationary distribution in place of $X(t)$, then $Y(t)$ becomes nearly constant after mixing, leading to degenerate ranking/classification diagnostics.

4.5 Decision Grid and Intervention Epochs

Operational decisions in maintenance and reliability management are typically taken at discrete inspection or monitoring instants rather than continuously over time. In the maintenance optimization and Markov decision process literature, such instants are referred to as *decision epochs* or *inspection epochs* [34,35]. Consistently with this framework, we introduce a discrete decision structure over the observation horizon.

Let

$$\mathcal{T} = \{t_1, t_2, \ldots, t_n\}, \qquad 0 < t_{k+1} - t_k < \Delta, \qquad k \in \{1, 2, \ldots, n-1\}$$

denote the *decision grid* as the ordered set of time instants at which the system state is observed and policy actions may be taken. In the empirical application, the grid coincides with the temporal resolution of the wind observations (hourly data), although the proposed formulation is not restricted to a particular sampling frequency.

At each decision epoch $t_k \in \mathcal{T}$, the wind-speed regime process is observed through the CTMC state

$$X(t_k) \in E,$$

and a policy signal is computed as a function of the observed state and the estimated generator matrix $\mathbf{Q}$. Formally, a policy signal is a state-dependent score of the form

$$S(t_k) = S\big(X(t_k)\big),$$

where $X(t_k)$ is the observed wind-speed regime state at decision time t_k. The signal therefore maps the currently observed regime into a scalar priority index, computed from the estimated transition structure of the CTMC. High values of $S(t_k)$ identify decision times that are considered more critical according to the selected indicator, and therefore more deserving of intervention under a limited budget. In this sense, the signal acts as the operational interface between the stochastic model and the ranking-based policy layer.

Thus, the decision grid serves two main purposes. First, it defines the admissible set of intervention times under a given policy. Second, it provides the evaluation sample used to assess policy performance. In particular, the short-horizon expected incremental loss defined in (33) is evaluated conditionally on the observed state at each decision epoch,

$$Y(t_k) = \mathbb{E}\left[\int_0^{\Delta} c\big(X(t_k + u)\big)\, \mathrm{d}u \,\middle|\, X(t_k) \right],$$

which represents the expected non-production exposure over the next operational horizon Δ.

Indicator-based policies can therefore be interpreted as *ranking or triggering rules* defined on the decision grid. At each epoch t_k, the signal $S(t_k)$ determines the priority assigned to that time window for inspection or intervention. Policy performance can then be evaluated using ranking-based metrics such as the AUC, the PR-curve and budget-constrained lift curves, which measure the fraction of expected loss captured when interventions are restricted to the highest-ranked decision epochs.

Since $X(t)$ is observed on a decision grid $\{t_k\}$ from the discretized wind-speed regime time series, we work with the state-conditional representation. For any $i \in E$,

$$Y_i(\Delta) := \mathbb{E}\left[\int_0^{\Delta} c\big(X(u)\big)\, \mathrm{d}u \,\middle|\, X(0) = i \right] = \int_0^{\Delta} \left(e_i\, e^{\mathbf{Q}u}\, c \right) \mathrm{d}u, \tag{34}$$

where e_i is the i-th canonical basis row vector and $c = (c(1), \dots, c(S))^{\top}$. Thus, on the decision grid, the realized target series is $Y(t_k) = Y_{X(t_k)}(\Delta)$ which certainly has nontrivial temporal variability under the state-conditional evaluation.

5 Indicator-Based Policies and Empirical Analysis

This Section consolidates the empirical analysis and the evaluation of indicator-based policies. The objective is not to redesign the physical model of wind dynamics, but to assess whether instantaneous mobility indicators extracted from an estimated CTMC generator provide actionable information for operational risk management. In particular, we investigate whether these indicators can (i) anticipate short-horizon non-production exposure, (ii) improve intervention efficiency under budget constraints, and (iii) support cross-site prioritization of wind assets.

5.1 What Is Being Tested: Indicators, Policies, and a Decision Problem

We consider a stylized decision setting: at discrete decision times t_k an operator may trigger an intervention (e.g., inspection, preventive maintenance, operational reconfiguration) subject to a limited *intervention budget*. The objective is to prioritize times (and, at a higher level, sites) where the *expected short-horizon non-production loss* is highest.

Accordingly, we compare alternative *policy signals* $S(t_k)$ used for ranking/triggering decisions:

- **Mobility-based signals** derived from the CTMC generator $\mathbf{Q}$:
  - The instantaneous exit intensity, TMR: $S(t_k) = \mathrm{TMR}(X(t_k)) = \lambda_{X(t_k)}$;

  - The net transition pressure toward non-operational regimes, Failure-drift: $S(t_k) = \mathrm{DRIFT}(X(t_k)) = \mathrm{ROCOF}(X(t_k)) - \mathrm{ROCOR}(X(t_k))$.
- **Benchmark (non-mobility) signal:**
  - The indicator of non-operational regimes, Unavailability: $S(t_k) = \mathbb{I}_{\{X(t_k) \in F\}}$.

The empirical analysis addresses three questions: (i) do these signals rank sites consistently with their short-horizon exposure, (ii) do they outperform benchmark signals under identical intervention constraints, and (iii) do they support site-level prioritization rules (e.g., selecting sites with highest TMR or drift exposure).

5.2 Policy Evaluation: Triggers and Performance Metrics

We now formalize the policy signals and the evaluation metrics used to produce the empirical policy figures. Let $W \subset E$ and $F \subset E$ denote the working and failure sets (as in Section 2). Define $\lambda_i := -q_{i,i}$.

State-conditional trigger signals.

At decision time t_k, signals are evaluated as functions of the observed state $i = X(t_k)$:

$$\mathrm{TMR}(i) = \lambda_i, \tag{35}$$

$$\mathrm{ROCOF}(i) = \mathbb{I}_W(i) \sum_{j \in F} q_{i,j}, \tag{36}$$

$$\mathrm{ROCOR}(i) = \mathbb{I}_F(i) \sum_{j \in W} q_{i,j}, \tag{37}$$

$$\mathrm{UNAVAIL}(i) = \mathbb{I}_F(i). \tag{38}$$

In the empirical analysis we use state-conditional versions of the instantaneous indicators. Specifically, at each decision time t_k the observed regime $X(t_k) = i$ defines the initial distribution $\alpha = e_i$.

The corresponding policies decision-grid series are $S(t_k) = S(X(t_k))$. The policies studied in the empirical analysis are based on the following signals:

- **TMR:** $S(t_k) = \lambda_{X(t_k)}$,
- **DRIFT:** $S(t_k) = \mathrm{ROCOF}(X(t_k)) - \mathrm{ROCOR}(X(t_k))$,
- **Unavailability:** $S(t_k) = \mathbb{I}_{\{X(t_k) \in F\}}$.

In particular, as regards the DRIFT quantity, at a decision time t_k, suppose the observed wind-speed regime is $X(t_k) = i$. The empirical instantaneous drift-failure is

$$\mathrm{DRIFT}(i) = \mathrm{ROCOF}(i) - \mathrm{ROCOR}(i) = \mathbb{I}_W(i) \sum_{j \in F} q_{i,j} - \mathbb{I}_F(i) \sum_{j \in W} q_{i,j}, \tag{39}$$

which for every t_k in the decision grid corresponds to $\mathrm{ROCOF}(i)$, if $X(t_k) = i \in W$, and to $-\mathrm{ROCOR}(i)$ if $X(t_k) = i \in F$. Eq. (39) represents the instantaneous rate at which the process exits the current regime toward the set of non-operational states F.

High-risk labeling (top-quantile rule).

For discrimination-based evaluation, define "high risk" times through a quantile threshold on the target. Fix $q \in (0, 1)$ and let τ_q be the empirical q-quantile of $\{Y(t_k)\}_{k=1}^{n}$. Define the binary label

$$Z(t_k) = \mathbb{I}_{\{Y(t_k) \geq \tau_q\}}. \tag{40}$$

In the empirical results, we use $q \in \{0.80, 0.90\}$ (top 10%–20% of $Y(t)$).

AUC and PR-curve (discrimination).

Given a score series $S(t_k)$ and labels $Z(t_k)$, the AUC is the probability that a randomly chosen (~) high-risk time t^+ receives a larger score than a randomly chosen non-high-risk time t^-:

$$\mathrm{AUC}(S) = \mathbb{P}(S(t^+) > S(t^-)), \qquad t^+ \sim \mathcal{T}^+ := \{k : Z(t_k) = 1\}, \ \ t^- \sim \mathcal{T}^- := \{k : Z(t_k) = 0\}. \tag{41}$$

The implementation uses the equivalent rank-based formulation (with tie handling via average ranks).

To construct a PR curve, it is necessary to compute two key quantities: Precision and Recall, defined as follows:

$$\text{Precision} = \frac{TP}{TP + FP}, \qquad \text{Recall} = \frac{TP}{TP + FN}, \tag{42}$$

where TP stands for true positives, FP false positives, and FN false negatives. These quantities can be calculated using the following formulas:

$$TP(\theta) = \sum_{k=1}^{n} \mathbb{I}_{\{S(t_k) \geq \theta\}} \mathbb{I}_{\{Z(t_k)=1\}}, \tag{43}$$

$$FP(\theta) = \sum_{k=1}^{n} \mathbb{I}_{\{S(t_k) \geq \theta\}} \mathbb{I}_{\{Z(t_k)=0\}}, \tag{44}$$

$$FN(\theta) = \sum_{k=1}^{n} \mathbb{I}_{\{S(t_k) < \theta\}} \mathbb{I}_{\{Z(t_k)=1\}}. \tag{45}$$

These measures are computed over varying decision threshold θ (in our case the q-quantile) to generate the PR curve. This allows us to analyze the trade-off between Precision and Recall as the decision threshold changes, see e.g., [36].

Lift (budgeted capture efficiency).

Let $t_{(1)}, \ldots, t_{(n)}$ denote decision times ordered by decreasing score, $S(t_{(1)}) \geq \cdots \geq S(t_{(n)})$.

Let define the parameter $b \in (0, 1]$ as the intervention budget, i.e., the fraction of decision times on which actions can be deployed. It therefore determines the proportion of top-ranked observations that can be selected for intervention under resource constraints.

Thus, the lift of signal S is

$$\mathrm{Lift}_S(b) = \frac{\sum_{m=1}^{\lfloor bn \rfloor} Y\big(t_{(m)}\big)}{\sum_{m=1}^{n} Y(t_m)}, \tag{46}$$

where $\lfloor x \rfloor$ denotes the floor operator, i.e., the greatest integer less than or equal to x. Thus $\lfloor bn \rfloor$ represents the number of decision times that can be acted upon when interventions are limited to a fraction b of the n total observations.

Eq. (46) measures the fraction of all positive events captured by the top b proportion of decision times ranked by the signal S. Equivalently, $\mathrm{Lift}_S(b)$ can be interpreted as a *budgeted capture efficiency*: given that only a fraction b of interventions can be deployed, it quantifies how many of the observed events are concentrated in the highest–scoring time points.

The metric belongs to the family of cumulative gain or lift measures widely used in predictive modeling and ranking evaluation [28,29]. In such settings, observations are sorted according to a score or predicted probability and the cumulative fraction of positives retrieved within the top quantiles of the ranking is analyzed to assess the model's ability to concentrate events in the highest-ranked subset of the population. This approach is common in credit scoring, marketing response modeling, fraud detection, and other resource-constrained decision problems where only a limited fraction of actions can be taken (e.g., contacting a subset of customers or triggering interventions).

Under random ranking, each event is equally likely to appear in any position of the ordered list; hence the expected fraction of events contained in the top b fraction of the sample equals b. Therefore the random baseline satisfies

$$\mathrm{Lift}(b) = b$$

Deviations above this line indicate that the score S successfully concentrates events in the highest-ranked observations, while curves close to the baseline indicate little or no predictive discrimination [28].

In practice, plotting $\mathrm{Lift}_S(b)$ as a function of b yields the *lift curve*, which provides a graphical diagnostic of how effectively the signal prioritizes intervention opportunities across different budget levels.

To clarify the logic of the empirical framework, it is useful to distinguish three connected layers, (see Fig. 1). The first is a *stochastic modeling layer*, where wind-speed observations are discretized into regimes and used to estimate the CTMC generator. The second is a *signal extraction layer*, where mobility-based indicators are computed from the estimated transition structure together with the operational mapping between working and failure states. The third is a *decision-analytics layer*, where the resulting signals are used to rank decision times and are evaluated against the short-horizon expected loss target through discrimination and budgeted capture metrics.

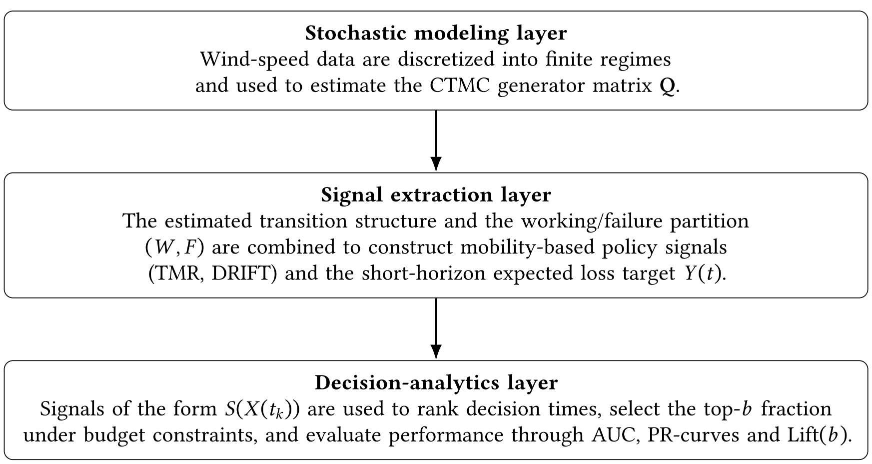

Figure 1: Three-layer representation of the empirical framework.

6 Indicator-Based Policies: Empirical Results

6.1 Data and State Construction

The empirical analysis uses hourly wind-speed time series collected at 50 m above ground level for a set of large wind farms distributed across heterogeneous climatic regions. Fig. 2 reports the geographical distribution of the selected locations.

Figure 2: Geographical distribution of the wind-farm sites considered in the empirical analysis.

For each site, wind speeds are discretized into a finite set of wind-regime states via a common partition shared across sites. Let $b_1 < \ldots < b_{S-1}$ denote fixed thresholds (common across sites) and define the discrete state process by

$$X_t = r \quad \Leftrightarrow \quad b_r < V_t \le b_{r+1}, \qquad r \in \{1, \ldots, S\},$$

with the usual conventions for the extreme bins. This common discretization ensures comparability across sites for both generator estimates and mobility indicators.

Weibull fits are computed only as descriptive benchmarks for marginal wind-speed distributions and are not used in CTMC estimation nor in the computation of mobility indicators. Fig. 3 reports histograms and fitted Weibull densities.

6.2 Estimation of the Generator Matrix

For each site, we estimate the CTMC generator $\mathbf{Q} = (q_{i,j})_{i,j \in E}$ from the discretized regime sequence using the standard two-step CTMC inference based on (i) empirical holding/sojourn times and (ii) embedded transition counts.

Let N_i denote the number of observed exits from state i in the sample path, and let T_i denote the total time spent in state i (over the observation window, measured in hours). Under exponential holding times, the maximum-likelihood estimator of the exit rate is

$$\widehat{\lambda}_i = \frac{N_i}{T_i}. \tag{47}$$

Equivalently, if $L_{i,1}, \ldots, L_{i,m_i}$ are the observed run lengths (in hours) for visits to state i, then $\widehat{\lambda}_i = 1/\overline{L_i}$.

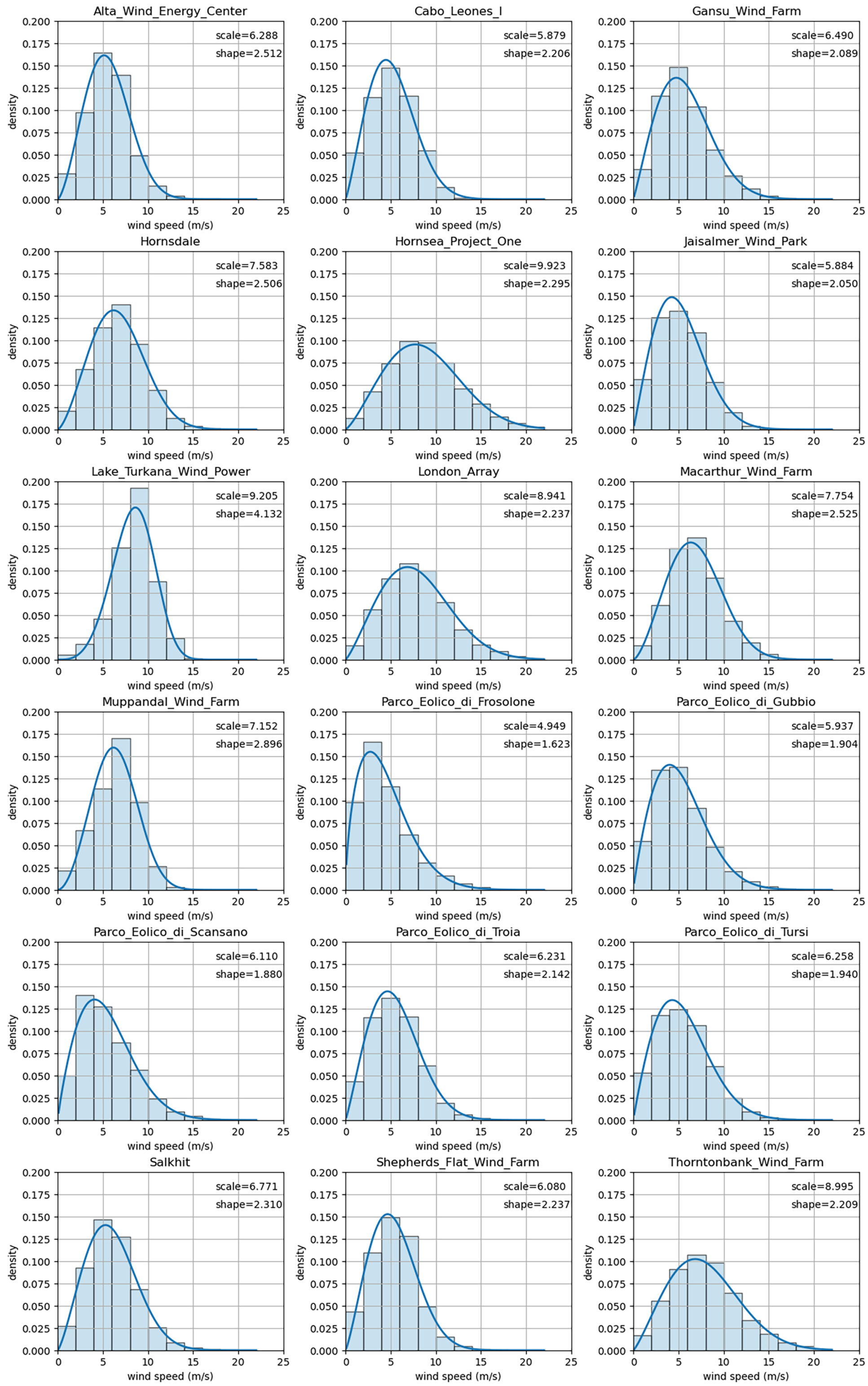

Figure 3: Empirical wind-speed distributions and fitted Weibull densities across sites (benchmark descriptive layer).

Next, let N_{ij} be the number of observed transitions from i to j with $j \neq i$. The embedded transition probabilities are

$$\widehat{p}_{i,j} = \frac{N_{i,j}}{\sum_{k \neq i} N_{i,k}}, \qquad j \neq i. \tag{48}$$

The generator estimator is then

$$\widehat{q}_{i,j} = \widehat{\lambda}_i \, \widehat{p}_{i,j}, \quad j \neq i, \qquad \widehat{q}_{i,i} = -\widehat{\lambda}_i, \tag{49}$$

which enforces the CTMC constraints by construction (nonnegative off-diagonals, row sums equal to zero).

In the present empirical implementation, the generator matrix $\widehat{\mathbf{Q}}$ is estimated on the entire available sample for each site; consequently, the subsequent analyses should be interpreted as in-sample, indicator-oriented diagnostics aimed at illustrating the ranking properties of the proposed mobility signals, rather than as out-of-sample predictive validation.

For diagnostics, we report the estimated embedded transition matrices $\widehat{\mathbf{P}}$ and the corresponding generators $\widehat{\mathbf{Q}}$ across sites (Figs. 4 and 5).

To improve the readability of the estimated transition structure, we report in Fig. 6 the numerical values of the estimated embedded transition matrix $\widehat{\mathbf{P}}$ and of the corresponding CTMC generator $\widehat{\mathbf{Q}}$ for the London Array site as an example.

6.3 From Indicators to Policies: AUC, PR and Lift Results

The empirical evaluation is conducted on two complementary layers. First, we assess the *time-local* performance of indicator-based policies, asking whether they correctly rank high-risk decision windows. Second, we move to a *structural, cross-site* perspective, where indicators are aggregated to support asset-level prioritization. This Subsection addresses the first layer.

We now assess the empirical performance of the candidate policy signals using the discrimination and capture-efficiency metrics introduced in Section 5.2. The objective is to evaluate whether instantaneous mobility indicators extracted from the estimated generator matrix provide actionable information for short-horizon non-production risk.

Discrimination performance (AUC and PR).

Figs. 7 and 8 report the distribution of AUC values across sites and the corresponding site-level realizations. The AUC measures the ability of a signal to correctly rank high-risk decision times—defined as the top 10%–20% of the short-horizon (6–8 h) expected loss $Y(t)$—above low-risk ones. An AUC close to 0.5 indicates no discriminative power beyond random ranking, while larger values reflect increasing predictive content. In the present context, a high AUC indicates that the indicator is well aligned with the conditional short-horizon loss induced by the CTMC dynamics, and therefore suitable as a triggering signal under partial observability.

The results highlight a clear separation between mobility-based and benchmark signals. Indicators associated with transitions across operational sets, in particular ROCOF and the DRIFT signal, achieve systematically higher AUC values across most sites. This indicates that periods characterized by elevated instantaneous transition intensity toward non-operational regimes are reliably associated with higher short-horizon exposure. In contrast, availability-based cluster around the random benchmark, suggesting limited usefulness for short-horizon prioritization.

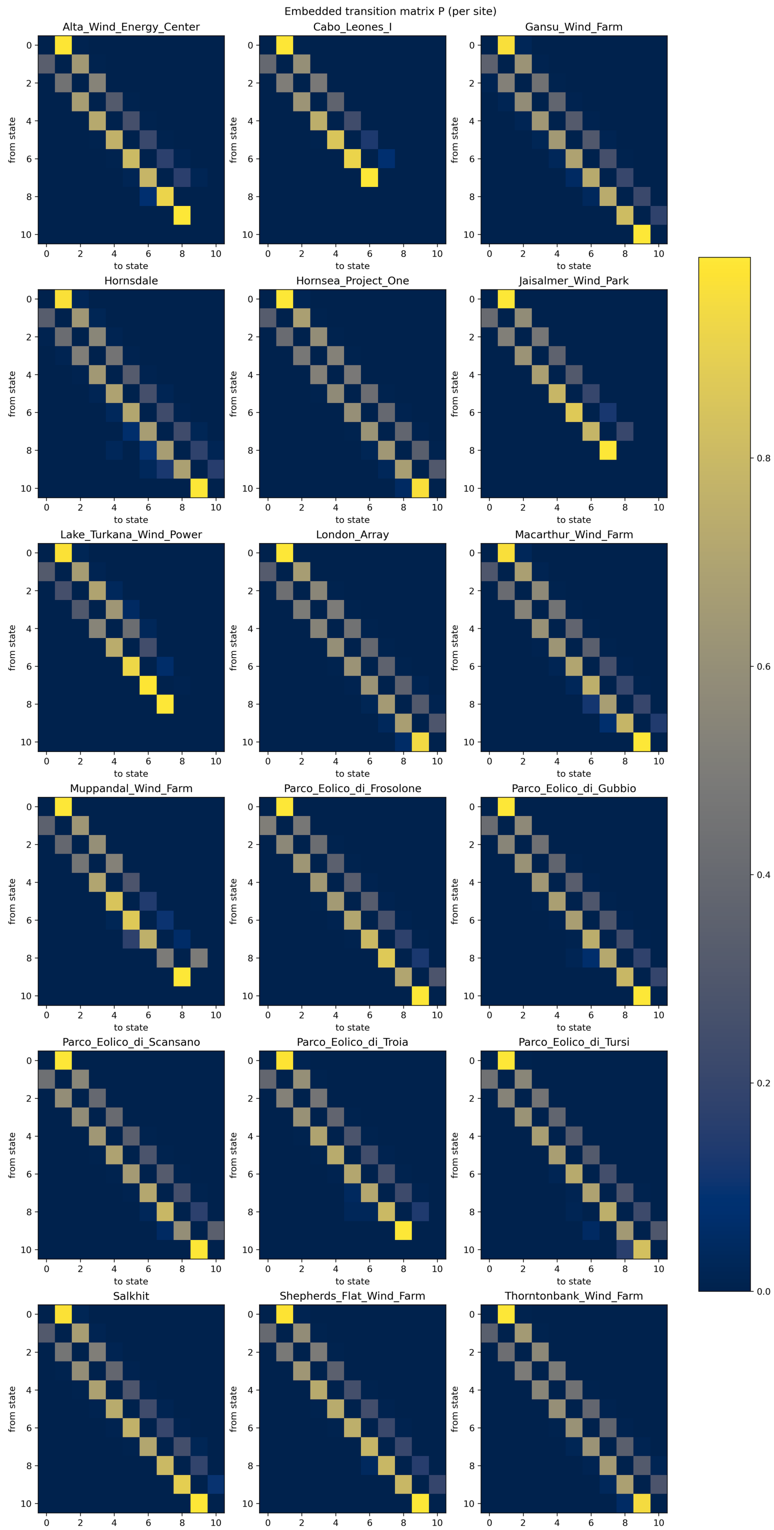

Figure 4: Estimated embedded transition matrices $\widehat{\mathbf{P}}$ by site.

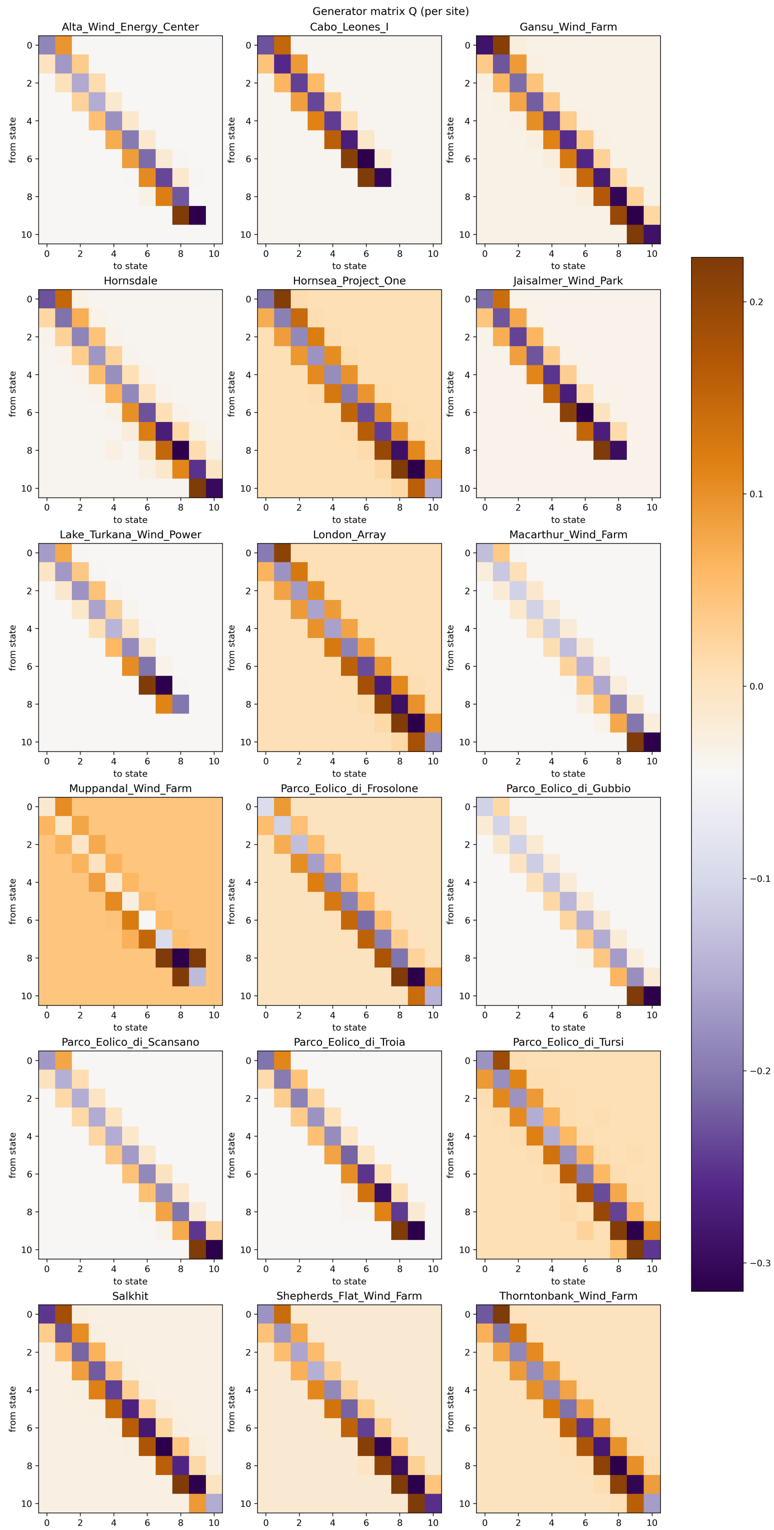

Figure 5: Estimated generator matrices $\widehat{\mathbf{Q}}$ by site.

Embedded transition matrix P — London Array

	State 1	State 2	State 3	State 4	State 5	State 6	State 7	State 8	State 9	State 10	State 11
State 1	0.0000	0.9951	0.0049	0.0000	0.0000	0.0000	0.0000	0.0000	0.0000	0.0000	0.0000
State 2	0.3258	0.0000	0.6699	0.0038	0.0005	0.0000	0.0000	0.0000	0.0000	0.0000	0.0000
State 3	0.0010	0.4344	0.0000	0.5590	0.0049	0.0003	0.0003	0.0000	0.0000	0.0000	0.0000
State 4	0.0000	0.0009	0.4953	0.0000	0.4986	0.0046	0.0006	0.0000	0.0000	0.0000	0.0000
State 5	0.0000	0.0000	0.0030	0.5433	0.0000	0.4498	0.0040	0.0000	0.0000	0.0000	0.0000
State 6	0.0000	0.0000	0.0000	0.0026	0.5986	0.0000	0.3923	0.0056	0.0009	0.0000	0.0000
State 7	0.0000	0.0000	0.0000	0.0000	0.0041	0.6245	0.0000	0.3627	0.0068	0.0020	0.0000
State 8	0.0000	0.0000	0.0000	0.0000	0.0000	0.0091	0.6193	0.0000	0.3591	0.0125	0.0000
State 9	0.0000	0.0000	0.0000	0.0000	0.0000	0.0000	0.0224	0.6578	0.0000	0.3116	0.0081
State 10	0.0000	0.0000	0.0000	0.0000	0.0000	0.0000	0.0000	0.0340	0.6766	0.0000	0.2894
State 11	0.0000	0.0000	0.0000	0.0000	0.0000	0.0000	0.0000	0.0000	0.0556	0.9444	0.0000

(**a**) Estimated transition matrix $\widehat{\mathbf{P}}$ for the London Array site.

Generator matrix Q — London Array

	State 1	State 2	State 3	State 4	State 5	State 6	State 7	State 8	State 9	State 10	State 11
State 1	-0.2094	0.2084	0.0010	0.0000	0.0000	0.0000	0.0000	0.0000	0.0000	0.0000	0.0000
State 2	0.0608	-0.1867	0.1251	0.0007	0.0001	0.0000	0.0000	0.0000	0.0000	0.0000	0.0000
State 3	0.0002	0.0779	-0.1793	0.1002	0.0009	0.0001	0.0001	0.0000	0.0000	0.0000	0.0000
State 4	0.0000	0.0002	0.0853	-0.1722	0.0859	0.0008	0.0001	0.0000	0.0000	0.0000	0.0000
State 5	0.0000	0.0000	0.0005	0.0941	-0.1732	0.0779	0.0007	0.0000	0.0000	0.0000	0.0000
State 6	0.0000	0.0000	0.0000	0.0005	0.1219	-0.2037	0.0799	0.0011	0.0002	0.0000	0.0000
State 7	0.0000	0.0000	0.0000	0.0000	0.0010	0.1544	-0.2473	0.0897	0.0017	0.0005	0.0000
State 8	0.0000	0.0000	0.0000	0.0000	0.0000	0.0027	0.1815	-0.2930	0.1052	0.0037	0.0000
State 9	0.0000	0.0000	0.0000	0.0000	0.0000	0.0000	0.0069	0.2019	-0.3069	0.0956	0.0025
State 10	0.0000	0.0000	0.0000	0.0000	0.0000	0.0000	0.0000	0.0113	0.2236	-0.3305	0.0956
State 11	0.0000	0.0000	0.0000	0.0000	0.0000	0.0000	0.0000	0.0000	0.0105	0.1789	-0.1895

(**b**) Estimated generator matrix $\widehat{\mathbf{Q}}$ for the London Array site.

Figure 6: Numerical representation of the estimated embedded transition matrix and generator matrix for the London Array site. The tables complement the heat maps by making the magnitudes of transition probabilities and transition intensities directly observable.

The dispersion observed in Fig. 8 further reveals substantial heterogeneity across sites. This heterogeneity is not explained by marginal wind-speed distributions alone, and instead reflects differences in the underlying transition dynamics encoded in the site-specific generators.

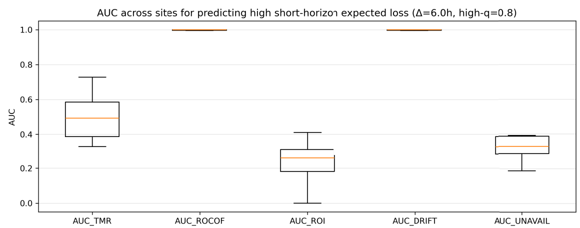

(**a**) High risk as the top 20% of $Y(t)$ with $\Delta = 6$ h

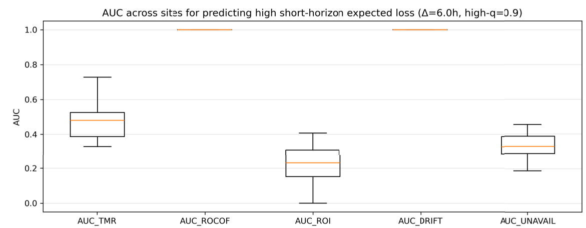

(**b**) High risk as the top 10% of $Y(t)$ with $\Delta = 6$ h

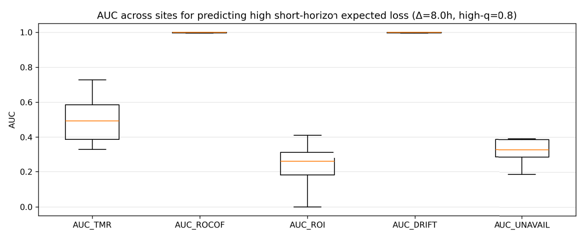

(**c**) High risk as the top 20% of $Y(t)$ with $\Delta = 8$ h

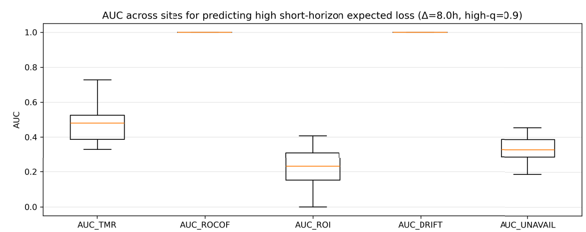

(**d**) High risk as the top 10% of $Y(t)$ with $\Delta = 8$ h

Figure 7: AUC across sites for predicting high short-horizon expected loss.

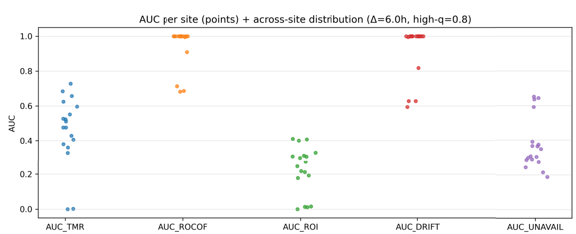

(**a**) Site-level AUC with $q = 80\%$ and $\Delta = 6$ h

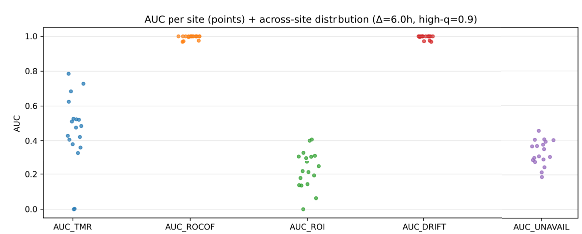

(**b**) Site-level AUC with $q = 90\%$ and $\Delta = 6$ h

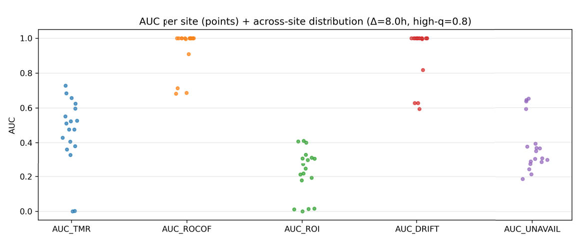

(**c**) Site-level AUC with $q = 80\%$ and $\Delta = 8$ h

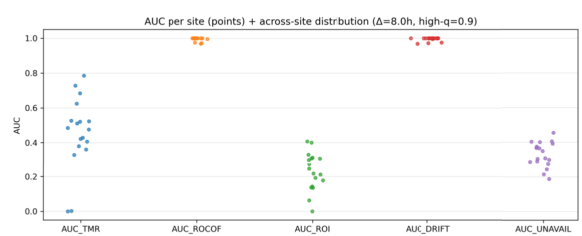

(**d**) Site-level AUC with $q = 90\%$ and $\Delta = 8$ h

Figure 8: Site-level AUC values by signal, highlighting cross-site heterogeneity.

We also evaluate the candidate signals through PR analysis. PR curves focus directly on the positive class, namely the decision epochs associated with the largest values of the short-horizon expected loss target $Y(t)$. This is particularly relevant in the present setting because high-risk epochs are defined through upper quantiles of $Y(t)$, and therefore represent a relatively small fraction of the evaluation sample. The resulting Average Precision values in Fig. 9 confirm the evidence obtained from AUC. ROCOF and DRIFT signals display the highest PR performance across the considered sites and high-risk quantiles. By contrast, the Unavailability benchmark exhibits lower AP values, consistent with its limited ability to distinguish short-horizon exposure beyond the current operational status. The PR results are therefore consistent with the AUC analysis while providing a more class-sensitive assessment of signal performance under rare high-risk conditions.

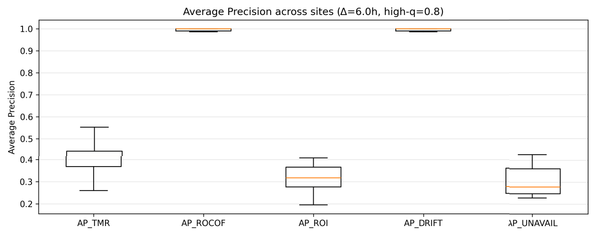

(**a**) Average Precision for $q = 0.8$ and $\Delta = 6$ h

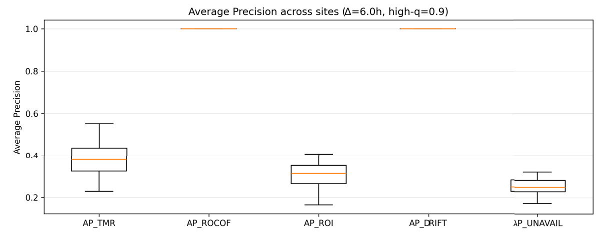

(**b**) Average Precision for $q = 0.9$ and $\Delta = 6$ h

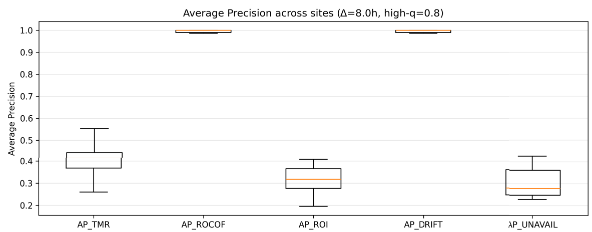

(**c**) Average Precision for $q = 0.8$ and $\Delta = 8$ h

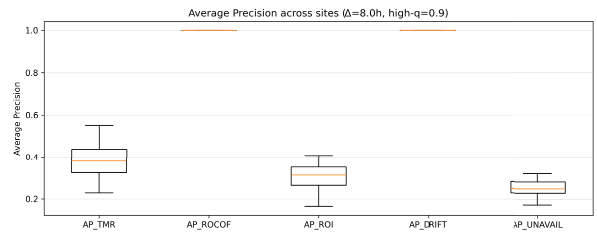

(**d**) Average Precision for $q = 0.9$ and $\Delta = 8$ h

Figure 9: Average Precision values by signal across sites.

Capture efficiency under budget constraints (lift).

While AUC evaluates ranking quality, operational decisions are subject to budget constraints. Lift curves therefore provide a complementary perspective by quantifying the fraction of total expected loss captured when interventions are triggered only at the highest-ranked time points. Lift therefore directly quantifies the operational value of a signal under resource constraints, translating ranking quality into expected loss reduction.

Fig. 10 reports mean lift curves across sites, together with interquartile bands and the random baseline. ROCOF and DRIFT overlap and dominate the random benchmark. In particular, ROCOF and DRIFT signal achieve the steepest initial lift, capturing a disproportionately large share of expected loss while acting on a limited fraction of decision times. Tables A1 and A2 in Appendix A summarize the statistical errors and confidence intervals associated with the lift curves.

By contrast, availability-based yield nearly linear lift curve, indicating weak concentration of exposure and limited operational relevance in short-horizon settings. These results confirm that instantaneous mobility indicators translate their discriminative power into tangible efficiency gains under realistic intervention constraints.

For completeness, the statistical errors associated with the lift curve estimates are reported in Appendix A. These additional tables complement the graphical evidence presented in this subsection and provide further support for assessing the robustness of the observed ranking performance. In particular, given the reported standard errors, the separation between the mobility-based signals, especially ROCOF and DRIFT, and the Unavailability benchmark remains visible across the considered intervention budgets, particularly for budgets $b > 0.1$.

Finally, we emphasize that this analysis is descriptive and indicator-oriented rather than inferential. AUC and lift curves are used to compare the ranking performance and operational usefulness of the proposed mobility-based indicators relative to benchmark signals, not to conduct formal hypothesis tests among competing statistical models. The results should therefore be interpreted as an assessment of relative prioritization ability under short-horizon risk-management objectives.

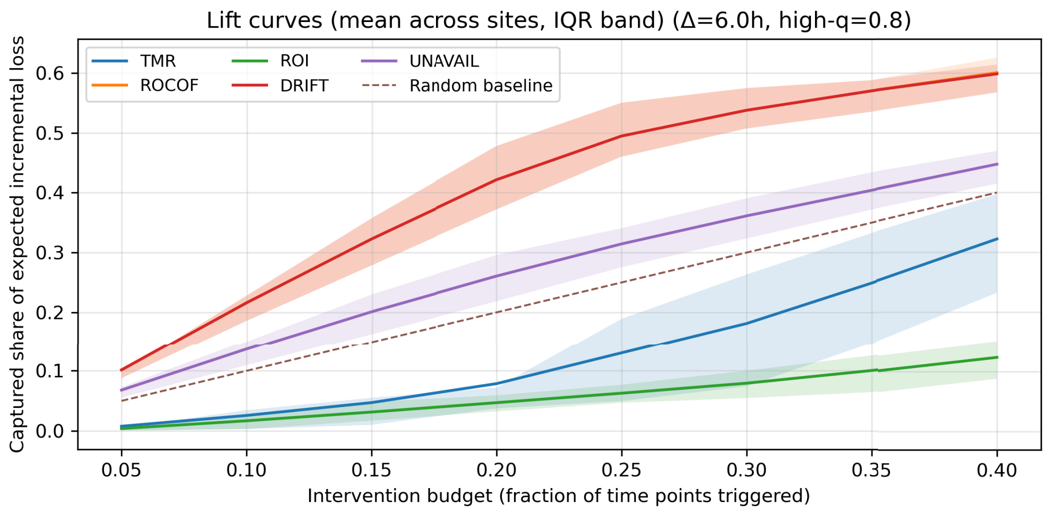

(**a**) Mean lift curves across sites for $\Delta = 6$ h and $q = 0.8$.

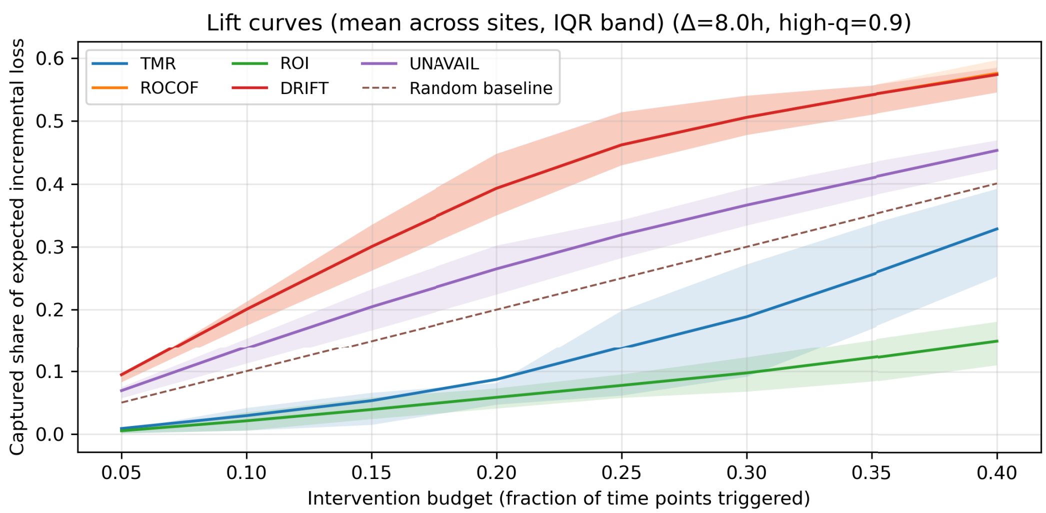

(**b**) Mean lift curves across sites for $\Delta = 8$ h and $q = 0.9$.

Figure 10: Lift curves: mean across sites with interquartile range band. The dashed line represents the random baseline. With a budget allowing intervention at 10% of time points ($b = 0.1$), the ROCOF signal captures ~20% of the expected losses, which is twice as effective as a random baseline (10%).

6.4 Cross-Site Risk Profiling and Site Selection

While the previous analysis focuses on time-local triggering decisions, risk management of wind assets also requires *structural, cross-site* prioritization. To address this problem, we use the integrated TMR (int_TMR) as a site-level descriptor of regime-switching intensity. Unlike ROCOF or DRIFT indicators, which are inherently local in time, int_TMR summarizes the cumulative dynamical instability of a site over the evaluation horizon.

In the empirical pipeline, $\mathrm{TMR}(t)$ is computed consistently from the CTMC via the identity $\mathrm{TMR}(t) = \sum_{i \in E} p_i(t)\lambda_i$, and then integrated numerically over $[0, H]$.

To connect structural mobility to short-horizon exposure, we compare int_TMR against the mean of the target process $Y(t)$. Fig. 11 shows the corresponding cross-site relationships.

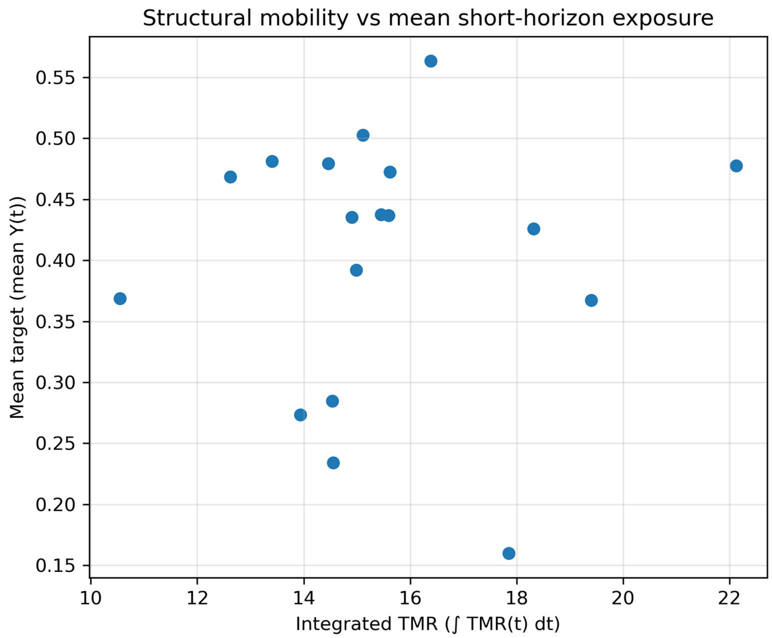

Figure 11: Mean of $Y(t)$: mean across sites of $Y(t)$ as a function of int_TMR(t).

These results support the fact that the mobility (and in particular int_TMR) captures a structural component of exposure linked to regime switching, which is not reducible to simple availability descriptors. This suggests a two-layer strategy: use integrated mobility for cross-site prioritization and monitoring allocation, and use event-directed signals (i.e., ROCOF and DRIFT) for time-local intervention triggers within selected sites.

For completeness, the main cross-site empirical summaries are reported in Table 2, included directly from the empirical pipeline.

Table 2: Site-level summary of mobility and non-production risk signals with H = 72 h.

Site	int_TMR	mean_TMR	E_L_E
Gansu_Wind_Farm	22.1283	0.3073	5.9274
Hornsdale	19.3996	0.2694	4.2666
Salkhit	18.3176	0.2544	5.5660
Lake_Turkana_Wind_Power	17.8540	0.2480	1.5709
Cabo_Leones_I	16.3868	0.2276	5.8952
Alta_Wind_Energy_Center	15.6230	0.2170	6.1542
Parco_Eolico_di_Troia	15.5944	0.2166	5.6095
Jaisalmer_Wind_Park	15.4527	0.2146	5.6370
Shepherds_Flat_Wind_Farm	15.1076	0.2098	5.8791
Macarthur_Wind_Farm	14.9834	0.2081	4.4778
Parco_Eolico_di_Tursi	14.9013	0.2070	5.2730
Hornsea_Project_One	14.5573	0.2022	2.7421
Thorntonbank_Wind_Farm	14.5358	0.2019	3.4052
Parco_Eolico_di_Scansano	14.4594	0.2008	5.6718
London_Array	13.9358	0.1936	3.4216

(Continued)

Table 2 (continued)

Site	int_TMR	mean_TMR	E_L_E
Parco_Eolico_di_Gubbio	13.4002	0.1861	5.9037
Parco_Eolico_di_Frosolone	12.6220	0.1753	5.7278
Muppandal_Wind_Farm	10.5472	0.1465	4.2558

7 Conclusions

This paper has developed a unified framework linking instantaneous mobility indicators of continuous-time Markov systems to short-horizon operational risk management in wind farms. Building on the theory of instantaneous failure, repair, and mobility rates [23,33], we have shifted the focus from structural reliability analysis to an explicitly decision-oriented perspective, in which mobility indicators serve as primitive signals for policy design under resource constraints.

At the modeling level, wind-speed regimes have been represented as a finite-state CTMC, while electrical production has been introduced as a deterministic output functional of the wind process. This separation between stochastic wind dynamics and operational consequences has allowed us to construct additive loss functionals for non-production exposure and to derive state-conditional short-horizon expected loss $Y(t)$ as a coherent policy target. In this setting, the ROCOF, the ROCOR, the ROI, and the TMR admit explicit representations in terms of the generator matrix and provide interpretable measures of instantaneous transition pressure.

The empirical analysis, conducted on a multi-site global dataset, demonstrates that mobility-based indicators contain actionable information for short-horizon non-production risk. In discrimination analysis, ROCOF and DRIFT signals systematically outperform availability ranking high-exposure decision windows. In operational terms, lift curves show that these indicators concentrate expected loss within a limited fraction of intervention opportunities, thereby delivering tangible efficiency gains under realistic budget constraints. The results are robust across heterogeneous climatic regimes and reveal that cross-site differences are primarily driven by transition dynamics rather than by marginal wind-speed distributions.

At the asset-allocation layer, integrated TMR emerges as a structural descriptor of site-level dynamical instability and correlates with average short-horizon exposure. This supports a two-layer risk-management strategy: mobility-based structural indicators for cross-site prioritization, and transition-directed signals (such as ROCOF or DRIFT) for time-local intervention triggering within selected sites.

Several directions for further research naturally arise. First, extensions to semi-Markov or non-homogeneous frameworks would allow for richer holding-time dynamics and seasonality effects. Second, the integration of price uncertainty and joint wind–price dependence would strengthen the revenue-risk dimension of the model. Third, the production functional could be refined by incorporating air-density normalization, which would improve the physical comparability of wind-speed-based production quantities across geographically heterogeneous wind farms, including mountain and offshore sites. Fourth, embedding the indicator-based rules into a fully dynamic stochastic control framework would permit formal optimality analysis under explicit intervention costs. Finally, coupling wind-speed regime mobility with mechanical failure processes could provide a more comprehensive representation of operational risk in wind assets.

Overall, the results suggest that instantaneous mobility indicators, originally developed within reliability theory, can be repurposed as effective tools for operational risk management in renewable energy systems. By translating structural transition information into actionable ranking signals, the framework bridges stochastic modeling and decision analytics, offering a principled approach to short-horizon risk-aware asset management.

Several directions for further research naturally arise. First, extensions to semi-Markov or non-homogeneous frameworks would allow for richer holding-time dynamics and seasonality effects. Second, a limitation of the present analysis is that the revenue-risk interpretation remains preliminary, since stochastic electricity prices and their dependence with wind regimes are not explicitly modeled. Future work should therefore integrate price uncertainty and joint wind–price dependence to strengthen the Revenue-at-Risk dimension of the framework. Importantly, this extension would not alter the proposed methodology, but would only require replacing the energy-loss rate with a price-adjusted loss functional incorporating the electricity price process. Third, the production functional could be refined by incorporating air-density normalization, which would improve the physical comparability of wind-speed-based production quantities across geographically heterogeneous wind farms, including mountain and offshore sites. Fourth, embedding the indicator-based rules into a fully dynamic stochastic control framework would permit formal optimality analysis under explicit intervention costs. Finally, coupling wind-speed regime mobility with mechanical failure processes could provide a more comprehensive representation of operational risk in wind assets.

Acknowledgement: None.

Funding Statement: Guglielmo D'Amico and Filippo Petroni acknowledge financial support from the European Union-NextGenerationEU program, Missione 4 Componente 1, CUP D53D23006470006, MUR PRIN 2022 n. 2022ETEHRM "Stochastic models and techniques for the management of wind farms and power systems" by the Italian Ministero dell'Universitá e della Ricerca.

Author Contributions: The authors confirm contribution to the paper as follows: Conceptualization, Guglielmo D'Amico and Filippo Petroni; methodology, Filippo Petroni; validation, Filippo Petroni and Edoardo Lui; formal analysis, Filippo Petroni and Edoardo Lui; investigation, Filippo Petroni and Edoardo Lui; data curation, Filippo Petroni and Edoardo Lui; writing—original draft preparation, Edoardo Lui; writing—review and editing, Guglielmo D'Amico and Filippo Petroni; visualization, Filippo Petroni and Edoardo Lui; supervision, Guglielmo D'Amico and Filippo Petroni; project administration, Guglielmo D'Amico; funding acquisition, Guglielmo D'Amico. All authors reviewed and approved the final version of the manuscript.

Availability of Data and Materials: The data described in this article have been downloaded from NASA POWER Project API: https://power.larc.nasa.gov/.

Ethics Approval: Not applicable.

Conflicts of Interest: The authors declare no conflicts of interest.

Appendix A Additional Results on Lift Curve Statistical Errors

This appendix reports the tables associated with the statistical errors of the lift curves discussed in Section 6.3. In particular, these tables complement the graphical analysis presented in Fig. 10, where the lift curves are used to compare the ranking performance of the proposed indicators.

The purpose of this appendix is to provide a more detailed numerical account of the uncertainty associated with the lift curve. While the Section 6.3 focuses on the visual comparison of the curves and on the interpretation of their relative performance, the tables reported here summarize the corresponding statistical errors, allowing for a more precise assessment of the stability and reliability of the observed patterns.

These additional results are intended to support the conclusions from the lift curve analysis without interrupting the flow of the main discussion.

Table A1: Standard error and 95% confidence intervals of lift-curve capture across sites for selected operational horizons and high-risk quantiles (Δ = 6 h, high-q = 0.80).

Δ (h)	High-q	Signal	Budget	N	Mean Capture	Std. Dev.	Std. Error	CI Low (95%)	CI High (95%)
6	0.80	TMR	0.05	18	0.0078	0.0146	0.0034	0.0031	0.0173
6	0.80	TMR	0.10	18	0.0258	0.0319	0.0075	0.0145	0.0446
6	0.80	TMR	0.15	18	0.0471	0.0528	0.0124	0.0285	0.0786
6	0.80	TMR	0.20	18	0.0787	0.0724	0.0171	0.0529	0.1206
6	0.80	TMR	0.25	18	0.1300	0.0976	0.0230	0.0922	0.1804
6	0.80	TMR	0.30	18	0.1814	0.1322	0.0312	0.1313	0.2500
6	0.80	TMR	0.35	18	0.2491	0.1592	0.0375	0.1916	0.3381
6	0.80	TMR	0.40	18	0.3224	0.1708	0.0403	0.2591	0.4154
6	0.80	ROCOF	0.05	18	0.1015	0.0315	0.0074	0.0927	0.1295
6	0.80	ROCOF	0.10	18	0.2164	0.0635	0.0150	0.1974	0.2664
6	0.80	ROCOF	0.15	18	0.3232	0.0746	0.0176	0.2957	0.3662
6	0.80	ROCOF	0.20	18	0.4217	0.0784	0.0185	0.3895	0.4615
6	0.80	ROCOF	0.25	18	0.4948	0.0580	0.0137	0.4686	0.5211
6	0.80	ROCOF	0.30	18	0.5379	0.0473	0.0111	0.5178	0.5608
6	0.80	ROCOF	0.35	18	0.5704	0.0441	0.0104	0.5530	0.5931
6	0.80	ROCOF	0.40	18	0.6007	0.0440	0.0104	0.5827	0.6226
6	0.80	ROI	0.05	18	0.0041	0.0095	0.0022	0.0016	0.0130
6	0.80	ROI	0.10	18	0.0169	0.0158	0.0037	0.0105	0.0247
6	0.80	ROI	0.15	18	0.0314	0.0186	0.0044	0.0230	0.0396
6	0.80	ROI	0.20	18	0.0470	0.0165	0.0039	0.0395	0.0543
6	0.80	ROI	0.25	18	0.0628	0.0198	0.0047	0.0543	0.0719
6	0.80	ROI	0.30	18	0.0794	0.0282	0.0066	0.0668	0.0923
6	0.80	ROI	0.35	18	0.1005	0.0362	0.0085	0.0838	0.1161
6	0.80	ROI	0.40	18	0.1242	0.0446	0.0105	0.1033	0.1429
6	0.80	DRIFT	0.05	18	0.1015	0.0315	0.0074	0.0927	0.1295
6	0.80	DRIFT	0.10	18	0.2164	0.0635	0.0150	0.1974	0.2664
6	0.80	DRIFT	0.15	18	0.3232	0.0746	0.0176	0.2957	0.3662
6	0.80	DRIFT	0.20	18	0.4217	0.0784	0.0185	0.3895	0.4615
6	0.80	DRIFT	0.25	18	0.4948	0.0580	0.0137	0.4686	0.5212
6	0.80	DRIFT	0.30	18	0.5379	0.0473	0.0112	0.5178	0.5608
6	0.80	DRIFT	0.35	18	0.5704	0.0441	0.0104	0.5530	0.5931
6	0.80	DRIFT	0.40	18	0.5986	0.0426	0.0100	0.5812	0.6201
6	0.80	UNAVAIL	0.05	18	0.0680	0.0254	0.0060	0.0553	0.0807
6	0.80	UNAVAIL	0.10	18	0.1364	0.0436	0.0103	0.1147	0.1581
6	0.80	UNAVAIL	0.15	18	0.2014	0.0512	0.0121	0.1759	0.2269
6	0.80	UNAVAIL	0.20	18	0.2607	0.0561	0.0132	0.2329	0.2885
6	0.80	UNAVAIL	0.25	18	0.3145	0.0606	0.0143	0.2843	0.3447
6	0.80	UNAVAIL	0.30	18	0.3614	0.0543	0.0128	0.3344	0.3884
6	0.80	UNAVAIL	0.35	18	0.4042	0.0545	0.0129	0.3770	0.4314
6	0.80	UNAVAIL	0.40	18	0.4475	0.0492	0.0116	0.4230	0.4720

Table A2: Standard error and 95% confidence intervals of lift-curve capture across sites for selected operational horizons and high-risk quantiles (Δ = 8 h, high-q = 0.90).

Δ (h)	High-q	Signal	Budget	N	Mean Capture	Std. Dev.	Std. Error	CI Low (95%)	CI High (95%)
8	0.90	TMR	0.05	18	0.0089	0.0150	0.0035	0.0040	0.0185
8	0.90	TMR	0.10	18	0.0293	0.0320	0.0075	0.0176	0.0474
8	0.90	TMR	0.15	18	0.0530	0.0519	0.0122	0.0341	0.0828
8	0.90	TMR	0.20	18	0.0868	0.0700	0.0165	0.0617	0.1269
8	0.90	TMR	0.25	18	0.1382	0.0913	0.0215	0.1030	0.1858
8	0.90	TMR	0.30	18	0.1888	0.1205	0.0284	0.1419	0.2492
8	0.90	TMR	0.35	18	0.2555	0.1445	0.0341	0.2018	0.3342
8	0.90	TMR	0.40	18	0.3276	0.1560	0.0368	0.2688	0.4108
8	0.90	ROCOF	0.05	18	0.0942	0.0277	0.0065	0.0865	0.1186
8	0.90	ROCOF	0.10	18	0.2010	0.0558	0.0131	0.1841	0.2445
8	0.90	ROCOF	0.15	18	0.3008	0.0670	0.0158	0.2758	0.3389
8	0.90	ROCOF	0.20	18	0.3929	0.0714	0.0168	0.3638	0.4293
8	0.90	ROCOF	0.25	18	0.4620	0.0532	0.0125	0.4383	0.4865
8	0.90	ROCOF	0.30	18	0.5058	0.0443	0.0104	0.4875	0.5277
8	0.90	ROCOF	0.35	18	0.5415	0.0420	0.0099	0.5253	0.5637
8	0.90	ROCOF	0.40	18	0.5755	0.0421	0.0099	0.5589	0.5973
8	0.90	ROI	0.05	18	0.0053	0.0106	0.0025	0.0025	0.0150
8	0.90	ROI	0.10	18	0.0211	0.0180	0.0043	0.0136	0.0298
8	0.90	ROI	0.15	18	0.0390	0.0212	0.0050	0.0291	0.0482
8	0.90	ROI	0.20	18	0.0584	0.0185	0.0044	0.0498	0.0663
8	0.90	ROI	0.25	18	0.0773	0.0224	0.0053	0.0674	0.0873
8	0.90	ROI	0.30	18	0.0971	0.0317	0.0075	0.0827	0.1112
8	0.90	ROI	0.35	18	0.1216	0.0405	0.0095	0.1029	0.1388
8	0.90	ROI	0.40	18	0.1487	0.0490	0.0116	0.1251	0.1688
8	0.90	DRIFT	0.05	18	0.0942	0.0277	0.0065	0.0865	0.1186
8	0.90	DRIFT	0.10	18	0.2010	0.0558	0.0131	0.1841	0.2445
8	0.90	DRIFT	0.15	18	0.3008	0.0670	0.0158	0.2758	0.3389
8	0.90	DRIFT	0.20	18	0.3929	0.0714	0.0168	0.3638	0.4293
8	0.90	DRIFT	0.25	18	0.4620	0.0532	0.0125	0.4383	0.4865
8	0.90	DRIFT	0.30	18	0.5058	0.0443	0.0104	0.4876	0.5277
8	0.90	DRIFT	0.35	18	0.5416	0.0420	0.0099	0.5253	0.5637
8	0.90	DRIFT	0.40	18	0.5735	0.0408	0.0096	0.5574	0.5948
8	0.90	UNAVAIL	0.05	18	0.0690	0.0255	0.0060	0.0563	0.0817
8	0.90	UNAVAIL	0.10	18	0.1387	0.0434	0.0102	0.1172	0.1602
8	0.90	UNAVAIL	0.15	18	0.2049	0.0510	0.0120	0.1796	0.2302
8	0.90	UNAVAIL	0.20	18	0.2649	0.0554	0.0131	0.2373	0.2925
8	0.90	UNAVAIL	0.25	18	0.3190	0.0591	0.0139	0.2897	0.3483
8	0.90	UNAVAIL	0.30	18	0.3663	0.0523	0.0123	0.3403	0.3923
8	0.90	UNAVAIL	0.35	18	0.4094	0.0519	0.0122	0.3837	0.4351
8	0.90	UNAVAIL	0.40	18	0.4527	0.0470	0.0111	0.4293	0.4761

References

1. Blischke WR, Murthy DNP. Reliability: modeling, prediction, and optimization. Hoboken, NJ, USA: John Wiley & Sons; 2011.
2. Ushakov I. Probabilistic reliability models. Hoboken, NJ, USA: John Wiley & Sons; 2012.
3. Barbu VS, Limnios N. Semi-Markov chains and hidden semi-Markov models toward applications: their use in reliability and DNA analysis, Vol. 191. New York, NY, USA: Springer Science & Business Media; 2009.
4. Lisnianski A, Levitin G. Multi-state system reliability: assessment, optimization and applications. Singapore, Singapore: World Scientific; 2003.
5. Koutras MV. On a Markov chain approach for the study of reliability structures. J Appl Probab. 1996;33(2):357–67.
6. Limnios N, Oprisan G. Semi-Markov processes and reliability. New York, NY, USA: Springer Science & Business Media; 2001.
7. Platis A, Limnios N, Le Du M. Dependability analysis of systems modeled by non-homogeneous Markov chains. Reliab Eng Syst Saf. 1998;61(3):235–49. doi:10.1016/s0951-8320(97)00073-2.
8. Limnios N. Dependability analysis of semi-Markov systems. Reliab Eng Syst Saf. 1997;55(3):203–7. doi:10.1016/s0951-8320(96)00121-4.
9. D'Amico G, Manca R, Petroni F, Selvamuthu D. On the computation of some interval reliability indicators for semi-Markov systems. Mathematics. 2021;9(5):575. doi:10.3390/math9050575.
10. Csenki A. On the interval reliability of systems modelled by finite semi-Markov processes. Microelectron Reliab. 1994;34(8):1319–35. doi:10.1016/0026-2714(94)90145-7.
11. Csenki A. An integral equation approach to the interval reliability of systems modelled by finite semi-Markov processes. Reliab Eng Syst Saf. 1995;47(1):37–45. doi:10.1016/0951-8320(94)00039-q.
12. Georgiadis S, Limnios N. Interval reliability for semi-Markov systems in discrete time. J De La Société Française De Stat. 2014;155(3):152–66.
13. Georgiadis S, Limnios N. Nonparametric estimation of interval reliability for discrete-time semi-Markov systems. J Stat Theory Pract. 2016;10(1):20–39. doi:10.1080/15598608.2015.1064049.
14. Barbu VS, D'Amico G, Gkelsinis T. Sequential interval reliability for discrete-time homogeneous semi-Markov repairable systems. Mathematics. 2021;9(16):1997. doi:10.3390/math9161997.
15. D'Amico G, Gkelsinis T. On a mixed transient–Asymptotic result for the sequential interval reliability for semi-Markov chains. Mathematics. 2024;12(12):1842. doi:10.3390/math12121842.
16. Yeh L. Calculating the rate of occurrence of failures for continuous-time Markov chains with application to a two-component parallel system. J Oper Res Soc. 1995;46(4):528–36. doi:10.1057/jors.1995.72.
17. Yeh L. Calculating the rate of occurrence of failures for a multistate system. IEEE Trans Reliab. 1995;44(1):22–7.
18. Yang K, Xue J. Continuous state reliability analysis. In: Proceedings of 1996 Annual Reliability and Maintainability Symposium; 1996 Jan 22–25; Las Vegas, NV, USA. p. 251–7.
19. Ouhbi B, Limnios N. The rate of occurrence of failures for semi-Markov processes and estimation. Stat Probab Lett. 2002;59(3):245–55. doi:10.1016/s0167-7152(02)00139-6.
20. Ouhbi B, Limnios N. Nonparametric reliability estimation of semi-Markov processes. J Stat Plan Inference. 2003;109(1–2):155–65. doi:10.1016/s0378-3758(02)00308-7.
21. D'Amico G. Rate of occurrence of failures (ROCOF) of higher-order for Markov processes: analysis, inference and application to financial credit ratings. Methodol Comput Appl Probab. 2015;17:929–49.
22. D'Amico G, Petroni F. ROCOF of higher order for semi-Markov processes. Appl Math Comput. 2023;441(3):127719. doi:10.1016/j.amc.2022.127719.
23. D'Amico G, Petroni F. Instantaneous failure, repair, and mobility rates for Markov reliability systems: a wind-farm application. Qual Reliab Eng Int. 2026;42(4):1496–514. doi:10.1002/qre.70151.
24. Clémençon S, Lugosi G, Vayatis N. Ranking and empirical minimization of u-statistics. Ann Stat. 2008;36(2):844–74. doi:10.1214/009052607000000910.
25. Morgoev I, Klyuev R, Morgoeva A. Methodology for detecting non-technical energy losses using an ensemble of machine learning algorithms. Comput Model Eng Sci. 2025;143(2):1381–99. doi:10.32604/cmes.2025.064502.

26. Chen YK, Bakhary N, Padil KH, Shamsudin MF, Ahmad A, Noh NH, et al. Efficient residual reliability criterion index in a permanent guided wave monitoring system. Measurement. 2022;197:111292. doi:10.1016/j.measurement.2022.111292.
27. Hanley JA, McNeil BJ. The meaning and use of the area under a receiver operating characteristic (ROC) curve. Radiology. 1982;143(1):29–36. doi:10.1148/radiology.143.1.7063747.
28. Fawcett T. An introduction to ROC analysis. Pattern Recognit Lett. 2006;27(8):861–74. doi:10.1016/j.patrec.2005.10.010.
29. Provost F, Fawcett T. Data science for business. Sebastopol, CA, USA: O'Reilly Media; 2013.
30. Rausand M, Høyland A. System reliability theory: models, statistical methods, and applications. New York, NY, USA: Wiley; 1994.
31. D'Amico G, Petroni F, Vergine S. Modelling and simulation of a storage system connected to a wind farm under ramp-rate limitation. Int J Model Simul. 2023;43(6):1021–40. doi:10.1080/02286203.2022.2147044.
32. Fazlizan A, Muzammil WK, Al-Khawlani NA. A review of computational fluid dynamics techniques and methodologies in vertical axis wind turbine development. Comput Model Eng Sci. 2025;144(2):1371. doi:10.32604/cmes.2025.067854.
33. D'Amico G, Masala G, Petroni F. Variability indexes for wind power. Discov Energy. 2025;5(1):13. doi:10.1007/s43937-025-00074-8.
34. Puterman ML. Markov decision processes: discrete stochastic dynamic programming. New York, NY, USA: John Wiley & Sons; 1994.
35. Castanier B, Grall A, Bérenguer C. A condition-based maintenance policy with non-periodic inspections for a two-unit series system. Reliab Eng Syst Saf. 2005;87(1):109–20. doi:10.1016/j.ress.2004.04.013.
36. Manning CD, Raghavan P, Schütze H. Introduction to information retrieval. Cambridge, UK: Cambridge University Press; 2008.